CHARTS FOR INTERPOLATION OF LOCAL SKIN FRICTION FROM EXPERIMENTAL TURBULENT VELOCITY PROFILES

ALLEN and TUDOR

NATIONAL AERONAUTICS AND SPACE ADMINISTRATION

NASA SP-3048

CHARTS FOR INTERPOLATION OF LOCAL SKIN FRICTION FROM EXPERIMENTAL TURBULENT VELOCITY PROFILES

By Jerry M. Allen and Dorothy H. Tudor
NASA Langley Research Center

Scientific and Technical Information Division
OFFICE OF TECHNOLOGY UTILIZATION 1969
NATIONAL AERONAUTICS AND SPACE ADMINISTRATION
Washington, D.C.

FOREWORD

Charts which allow the easy and rapid determination of local skin friction from experimental turbulent velocity profiles taken in air on smooth surfaces are presented. The charts, calculated from the Fenter-Stalmach law of the wall, cover a Mach number range from 0 to 5 and are good for all Reynolds numbers and total-temperature levels. Caution should be employed when using these charts with profiles taken under conditions of large heat transfer or pressure gradient because of the lack of reliable experimental verification of the theory under these test conditions. The use of these charts requires that the experimental profile be plotted on translucent paper to the same scale as the charts presented in this report and overlaid on to the proper chart.

INTRODUCTION

The most practical aspect of the compressible law-of-the-wall theory is that it allows the graphical interpolation of local skin friction from compressible velocity profiles. A recent NASA publication (ref. 1) has shown that two such theories, Baronti-Libby (ref. 2) and Fenter-Stalmach (ref. 3), give good results over the supersonic Mach number range, and that the necessity of hand plotting the data and theory could be eliminated by programing these law-of-the-wall methods on a high-speed digital computer. Without computer help, however, these methods are tedious to apply because of the lengthy calculations involved. The Baronti-Libby method, for example, requires different theory curves for each local free-stream Mach number and integration of the experimental velocity profile. The Fenter-Stalmach method also requires different theory curves for each Mach number. These curves are not linear for compressible flow; thus, many calculations are involved in order to obtain them. This method, however, requires no integration of the velocity profile, and thereby the experimental data are easier to handle than in the Baronti-Libby method.

Since the tedious part of using the Fenter-Stalmach law is calculating and plotting the theory curves, this paper presents these curves in convenient graphical form for a wide range of test conditions. All that is required to use these curves is to plot the experimental profile on translucent graph paper which has the same scale as the figures reproduced in this paper. (The scale used herein is the same as that obtained on commercially available graph paper.) Overlaying the experimental profile on to the proper figure allows the graphical interpolation of local skin friction by the Fenter-Stalmach law.

SYMBOLS

C_f	local skin-friction coefficient, $\frac{\tau_w}{\frac{1}{2}\rho_e u_e^2}$
$f(\eta)$	Coles' incompressible law-of-the-wall function (see table I)
M	Mach number
R	unit Reynolds number, $\frac{\rho_e u_e}{\mu_e}$
R_y	Reynolds number based on y, $\frac{\rho_e u_e y}{\mu_e}$
T	absolute temperature
u	velocity in longitudinal direction
y	vertical distance from wall
γ	ratio of specific heats (1.4 for air)
η	normal coordinate in law-of-the-wall profile, $\frac{y\rho_w}{\mu_w}\sqrt{\frac{\tau_w}{\rho_w}}$
μ	viscosity
ρ	density
σ	compressibility function in Fenter-Stalmach law of the wall, $\frac{\frac{\gamma - 1}{2} M_e^2}{1 + \frac{\gamma - 1}{2} M_e^2}$
τ	shearing stress

Subscripts:

aw	adiabatic wall conditions
e	edge of boundary-layer conditions

t free-stream stagnation conditions

w wall conditions

DISCUSSION

Fenter-Stalmach Law of the Wall

The Fenter-Stalmach law of the wall is given by equation (11) of reference 3 as

$$\frac{u_e}{\sqrt{\frac{\tau_w}{\rho_w}}\sqrt{\sigma}} \sin^{-1}\left(\sqrt{\sigma}\,\frac{u}{u_e}\right) = f(\eta) \tag{1}$$

where

$$\eta = \frac{y\rho_w}{\mu_w}\sqrt{\frac{\tau_w}{\rho_w}} \tag{2}$$

The function $f(\eta)$ is Coles' incompressible law of the wall (see ref. 4) and is reproduced in table I.

Making use of the definition of local skin-friction coefficient results in

$$\sqrt{\frac{\tau_w}{\rho_w}} = \sqrt{\frac{\rho_e}{\rho_w}}\sqrt{\frac{C_f}{2}}\,u_e \tag{3}$$

Using equation (3) in equations (1) and (2) yields

$$\sqrt{\frac{\rho_w}{\rho_e}}\sqrt{\frac{2}{C_f}}\,\frac{\sin^{-1}\left(\sqrt{\sigma}\,\frac{u}{u_e}\right)}{\sqrt{\sigma}} = f(\eta) \tag{4}$$

and

$$\eta = \frac{y\rho_w u_e}{\mu_w}\sqrt{\frac{\rho_e}{\rho_w}}\sqrt{\frac{C_f}{2}} \tag{5}$$

or, rearranging equation (4) yields

$$\frac{u}{u_e} = \frac{\sin\left[\sqrt{\sigma} f(\eta)\sqrt{\frac{C_f}{2}}\sqrt{\frac{\rho_e}{\rho_w}}\right]}{\sqrt{\sigma}} \tag{6}$$

and rewriting equation (5) yields

$$\eta = \frac{y\rho_e u_e}{\mu_e}\,\frac{\mu_e}{\mu_w}\sqrt{\frac{\rho_w}{\rho_e}}\sqrt{\frac{C_f}{2}} \tag{7}$$

Assuming constant static pressure across the boundary layer gives

$$\frac{\rho_w}{\rho_e} = \frac{T_e}{T_w} \tag{8}$$

Also, by definition

$$R_y = \frac{y\rho_e u_e}{\mu_e} \tag{9}$$

Therefore, equations (6) and (7) become

$$\frac{u}{u_e} = \frac{\sin}{\sqrt{\sigma}}\left[\sqrt{\sigma}\, f(\eta)\, \sqrt{\frac{C_f}{2}}\sqrt{\frac{T_w}{T_e}}\right] \tag{10}$$

and

$$\eta = \frac{\mu_e}{\mu_w} R_y \sqrt{\frac{T_e}{T_w}}\sqrt{\frac{C_f}{2}} \tag{11}$$

Reference 1 reports that the Fenter-Stalmach law does not yield good results under large heat-transfer conditions and that better results were obtained if the nonadiabatic profiles were assumed to be adiabatic. This paper therefore makes the assumption that adiabatic conditions exist; this assumption results in $\frac{T_w}{T_e} = \frac{T_{aw}}{T_e} = 1 + 0.176M_e^2$ for $\gamma = 1.4$ and a turbulent recovery factor of 0.88. Inserting these values and the definition of σ into equations (10) and (11) results in

$$\frac{u}{u_e} = \frac{\sqrt{5 + M_e^2}}{M_e} \sin\left[\frac{M_e\sqrt{1 + 0.176M_e^2}}{\sqrt{10 + 2M_e^2}}\, f(\eta)\, \sqrt{C_f}\right] \tag{12}$$

and

$$\frac{\mu_e}{\mu_w} R_y = \frac{\sqrt{2 + 0.352M_e^2}}{\sqrt{C_f}}\, \eta \tag{13}$$

Scales Used for Plots

The left-hand side of equations (12) and (13) were used as the Fenter-Stalmach parameters. The viscosity ratio μ_e/μ_w was included in the second parameter so that the plots would be independent of the total-temperature level. Plots of the Fenter-Stalmach law were prepared from Mach 0 to 5 in increments of 0.2 and are presented in figures 1 to 26. These charts were plotted on semi-log paper, the scale of the ordinate u/u_e being 0.0 to 1.0 covering 5 inches (127.0 mm) of grid, and the scale of the abscissa $\frac{\mu_e}{\mu_w} R_y$ being 2-inch (50.8 mm) log cycles. This size of graph paper is commercially available.

Viscosity Ratio

The use of this technique requires that the experimental velocity profile be used in the form of the variation of u/u_e with $\frac{\mu_e}{\mu_w} R_y$. The viscosity ratio can be calculated from Sutherland's viscosity law as

$$\frac{\mu_e}{\mu_w} = \left(\frac{T_e}{T_w}\right)^{1.5} \frac{T_w + 199}{T_e + 199} \tag{14}$$

where T_w and T_e are in degrees Rankine. By assuming adiabatic conditions and a turbulent recovery factor of 0.88, equation (14) can be written as

$$\frac{\mu_e}{\mu_w} = \frac{\mu_e}{\mu_{aw}} = \frac{T_t + 0.176M_e^2T_t + 199 + 39.8M_e^2}{\left(1 + 0.176M_e^2\right)^{1.5}\left(T_t + 199 + 39.8M_e^2\right)} \tag{15}$$

Equation (15) has been used in preparing figure 27, which allows the rapid determination of the viscosity ratio for the test conditions of the experimental velocity profile.

Sample Profile

To illustrate the use of the plots presented in this paper, the sample profile used in reference 1 is presented in table II. The local free-stream conditions of this profile are $M_e = 2.20$, $R = 0.1764 \times 10^6/\text{cm}$, and $T_t = 316^\circ\text{ K} = 570^\circ\text{ R}$.

From figure 27, the viscosity ratio μ_e/μ_w is found to be approximately 0.600, which yields $\frac{\mu_e}{\mu_w} R$ to be $0.1058 \times 10^6/\text{cm}$. The parameter $\frac{\mu_e}{\mu_w} R_y$ can now be calculated from the experimental profile and is also listed in table II.

Figure 28 shows this profile superimposed over the theory curves of figure 12, which are the curves for $M_e = 2.20$. The skin friction for this profile is determined from data for which C_f is relatively constant, that is, from the data which are parallel to the theory curves. This region is easy to detect in this profile and yields a local skin-friction coefficient, determined by interpolation between the theory curves, of approximately 0.001430. Also shown in this figure is the value of C_f (0.001404) which was measured for the same test conditions by a skin-friction balance.

This sample profile has an edge Mach number of 2.20, which happens to be the same as one of the charts presented in this paper. For profiles taken at Mach numbers between these charts, interpolation between the two closest Mach numbers can be performed.

It can be seen from figure 28 that the range of data which is parallel to the theory curves is relatively small compared with the total amount of data in the profile. The data above this parallel region are outside the range of validity of the law of the wall and therefore would not be expected to yield constant skin-friction values. The reason the data below this region are not parallel is less clear since, in theory, the region of applicability

of the law of the wall should extend all the way through the lower part of the boundary layer to the wall. It is believed that the characteristic exhibited is probably due to experimental inaccuracies that are magnified as the wall is approached.

Limitations of Technique

The abscissa used here $\frac{\mu_e}{\mu_w} R_y$ was chosen so that no restrictions would be placed on the Reynolds number and total-temperature ranges of applicability of this technique. The plots contained in this paper cover a Mach number range from 0 to 5. The law of the wall has been used at higher Mach numbers (ref. 5, for example), but only in the supersonic Mach number range is enough data available to give confidence in the Fenter-Stalmach law as a skin-friction-measuring technique.

Other restrictions which are placed on this technique are as follows:

(1) The fluid medium must be air since a γ of 1.4 was used in this paper.

(2) The test surface on which the velocity profile is obtained must be "smooth" in the aerodynamic sense. Surface roughness changes the basic law of the wall (ref. 6, for example); therefore, the Fenter-Stalmach law could not be expected to give good results on rough surfaces.

(3) Caution should be employed in using this technique with profiles taken under conditions of large heat transfer. From the limited amount of cold-wall data available, reference 1 reported large differences between the measured skin friction and that calculated from velocity profiles using the Fenter-Stalmach law. The disagreement was as much as 70 percent at a T_w/T_{aw} value of about 0.6. Assuming the profiles to be adiabatic improved the agreement somewhat, the maximum difference being reduced to about 40 percent. This value is still much larger, however, than the ±5-percent disagreement which was obtained (ref. 1) from the large amount of adiabatic wall data available.

(4) Also, caution should be employed in using this technique with profiles taken in flows with large pressure gradients. The incompressible law of the wall has been shown to be valid in pressure gradient flow. (See ref. 7, for example.) It could be expected, therefore, that a compressible law of the wall, such as the Fenter-Stalmach law, also would be valid under pressure gradient conditions. Little experimental evidence is available, however, to verify this assumption.

CONCLUDING REMARKS

Charts are presented which allow the easy and rapid determination of local skin friction from experimental turbulent velocity profiles taken in air on smooth surfaces.

The charts, calculated from the Fenter-Stalmach law of the wall, cover a Mach number range from 0 to 5 and are good for all Reynolds numbers and total-temperature levels. Caution should be employed when using these charts with profiles taken under conditions of large heat transfer or pressure gradient because of the lack of reliable experimental verification of the theory under these test conditions. The use of these charts requires that the experimental profile be plotted on translucent paper to the same scale as the charts presented in this report and overlaid on to the proper chart.

REFERENCES

1. Allen, Jerry M.: Use of Baronti-Libby Transformation and Preston Tube Calibrations To Determine Skin Friction From Turbulent Velocity Profiles. NASA TN D-4853, 1968.

2. Baronti, Paolo O.; and Libby, Paul A.: Velocity Profiles in Turbulent Compressible Boundary Layers. AIAA J., vol. 4, no. 2, Feb. 1966, pp. 193-202.

3. Fenter, Felix W.; and Stalmach, Charles J., Jr.: The Measurement of Local Turbulent Skin Friction at Supersonic Speeds by Means of Surface Impact Pressure Probes. DRL 392, CM-878 (Contract NOrd-16498), Univ. of Texas, Oct. 21, 1957.

4. Coles, Donald: Measurements in the Boundary Layer on a Smooth Flat Plate in Supersonic Flow. Jet Propulsion Lab., California Inst. Technol.
   I. The Problem of the Turbulent Boundary Layer. Rep. No. 20-69 (Contract No. DA-04-495-Ord 18), June 1, 1953.
   II. Instrumentation and Experimental Techniques at the Jet Propulsion Laboratory. Rep. No. 20-70 (Contract No. DA-04-495-Ord 18), June 1, 1953.
   III. Measurements in a Flat-Plate Boundary Layer at the Jet Propulsion Laboratory. Rep. No. 20-71 (Contract No. DA-04-495-Ord 18), June 1, 1953.

5. Bertram, Mitchel H.; Cary, Aubrey M., Jr.; and Whitehead, Allen H., Jr.: Experiments With Hypersonic Turbulent Boundary Layers on Flat Plates and Delta Wings. Paper presented at AGARD Specialists' Meeting on Hypersonic Boundary Layers and Flow Fields (London, England), May 1-3, 1968.

6. Hama, Francis R.: Boundary-Layer Characteristics for Smooth and Rough Surfaces. Trans. Soc. Naval Architects and Marine Engrs., vol. 62, 1954, pp. 333-358.

7. Ludwieg, H.; and Tillmann, W.: Investigations of the Wall-Shearing Stress in Turbulent Boundary Layers. NACA TM 1285, 1950.

TABLE I.- COLES' INCOMPRESSIBLE LAW OF THE WALL

$$\left[\frac{u}{\sqrt{\frac{\tau_w}{\rho}}} = f(\eta) \quad \text{(ref. 4)}\right]$$

η	$f(\eta)$	η	$f(\eta)$
0	0	44	14.51
1	.99	50	14.87
2	1.96	60	15.33
3	2.90	80	16.04
4	3.80	100	16.60
5	4.65	150	17.61
6	5.45	200	18.33
7	6.19	300	19.34
8	6.87	400	20.06
9	7.49	500	20.62
10	8.05	600	21.08
12	9.00	800	21.79
14	9.76	1 000	22.35
16	10.40	1 500	23.36
18	10.97	2 000	24.08
20	11.49	3 000	25.09
24	12.34	4 000	25.81
28	12.99	5 000	26.37
32	13.48	6 000	26.83
36	13.88	8 000	27.54
40	14.22	10 000	28.10

TABLE II.- SAMPLE VELOCITY PROFILE

y, cm	$\frac{\mu_e}{\mu_w} R_y$	$\frac{u}{u_e}$	y, cm	$\frac{\mu_e}{\mu_w} R_y$	$\frac{u}{u_e}$
0.0114	1.206×10^3	0.5468	0.7277	7.699×10^4	0.8018
.0165	1.746	.5623	.8547	9.043	.8135
.0216	2.285	.5764	1.0071	1.066×10^5	.8297
.0266	2.814	.5870	1.1595	1.227	.8432
.0368	3.893	.6028	1.3500	1.428	.8592
.0455	4.814	.6163	1.5151	1.603	.8709
.0546	5.777	.6276	1.7056	1.805	.8860
.0673	7.120	.6405	1.8961	2.006	.8982
.0800	8.464	.6515	2.0866	2.208	.9128
.0927	9.808	.6604	2.2771	2.409	.9223
.1181	1.249×10^4	.6776	2.5311	2.678	.9376
.1434	1.517	.6912	2.7978	2.960	.9527
.1687	1.785	.7013	3.0518	3.229	.9649
.1943	2.056	.7114	3.3058	3.498	.9749
.2196	2.323	.7197	3.5598	3.766	.9836
.2578	2.728	.7296	3.8138	4.035	.9885
.3085	3.264	.7410	4.1948	4.438	.9925
.3722	3.938	.7531	4.8298	5.110	.9969
.4483	4.743	.7649	5.5918	5.916	.9991
.5245	5.549	.7768	6.3538	6.722	1.0003
.6134	6.490	.7884	7.1158	7.529	1.0000

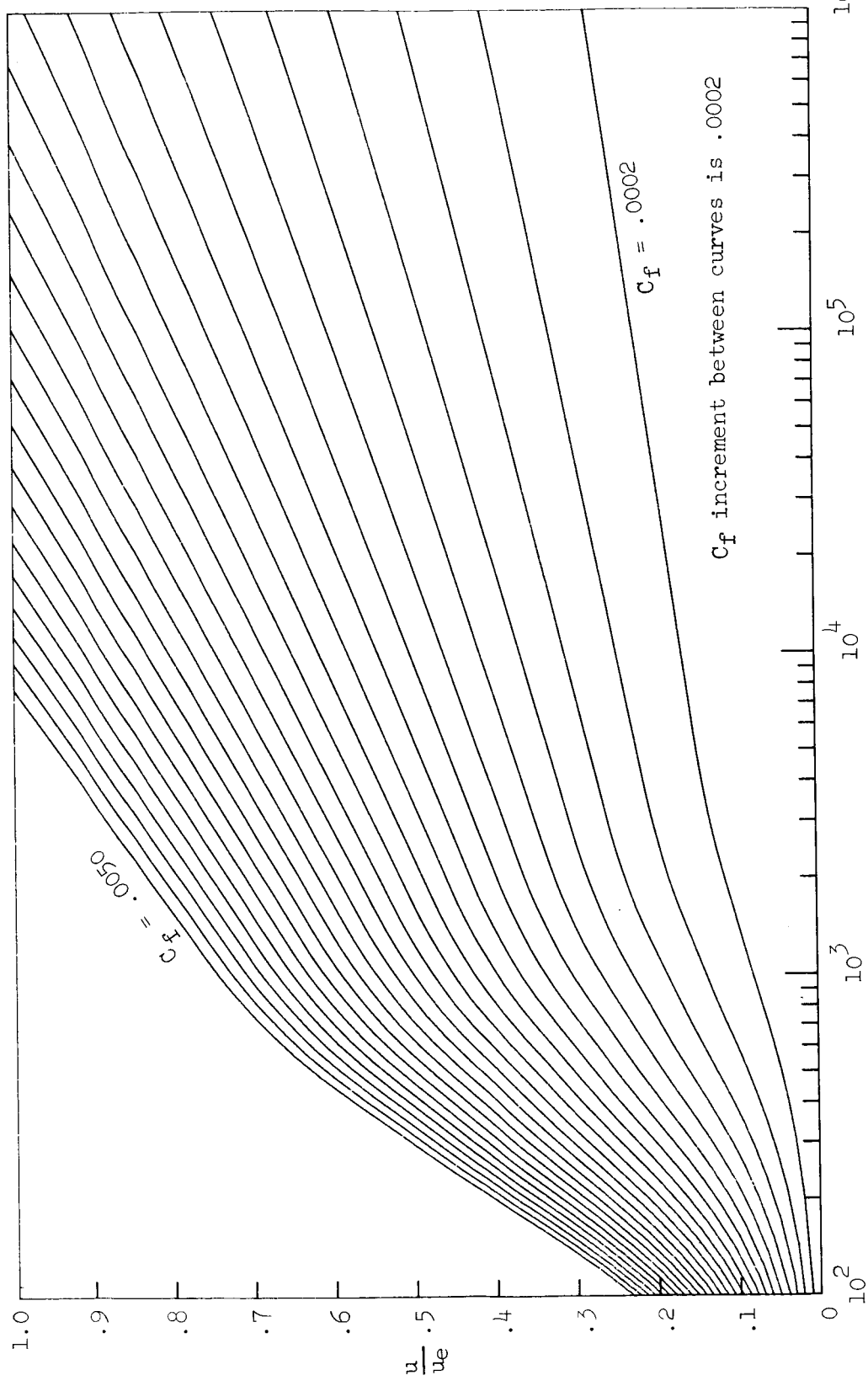

Figure 1.- Curves for interpolation of local skin-friction coefficients at $M_e = 0.00$.

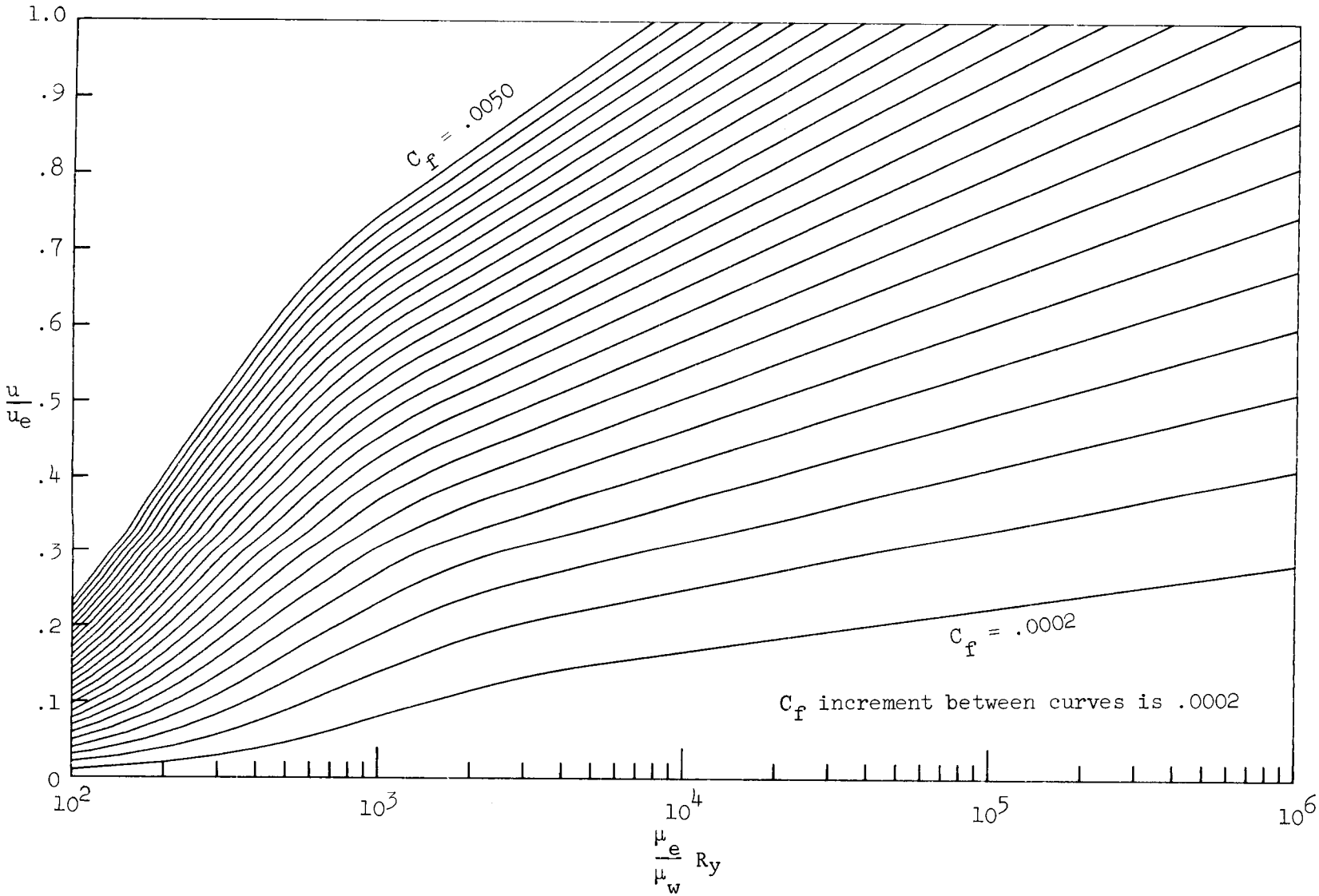

Figure 2.- Curves for interpolation of local skin-friction coefficients at $M_e = 0.20$.

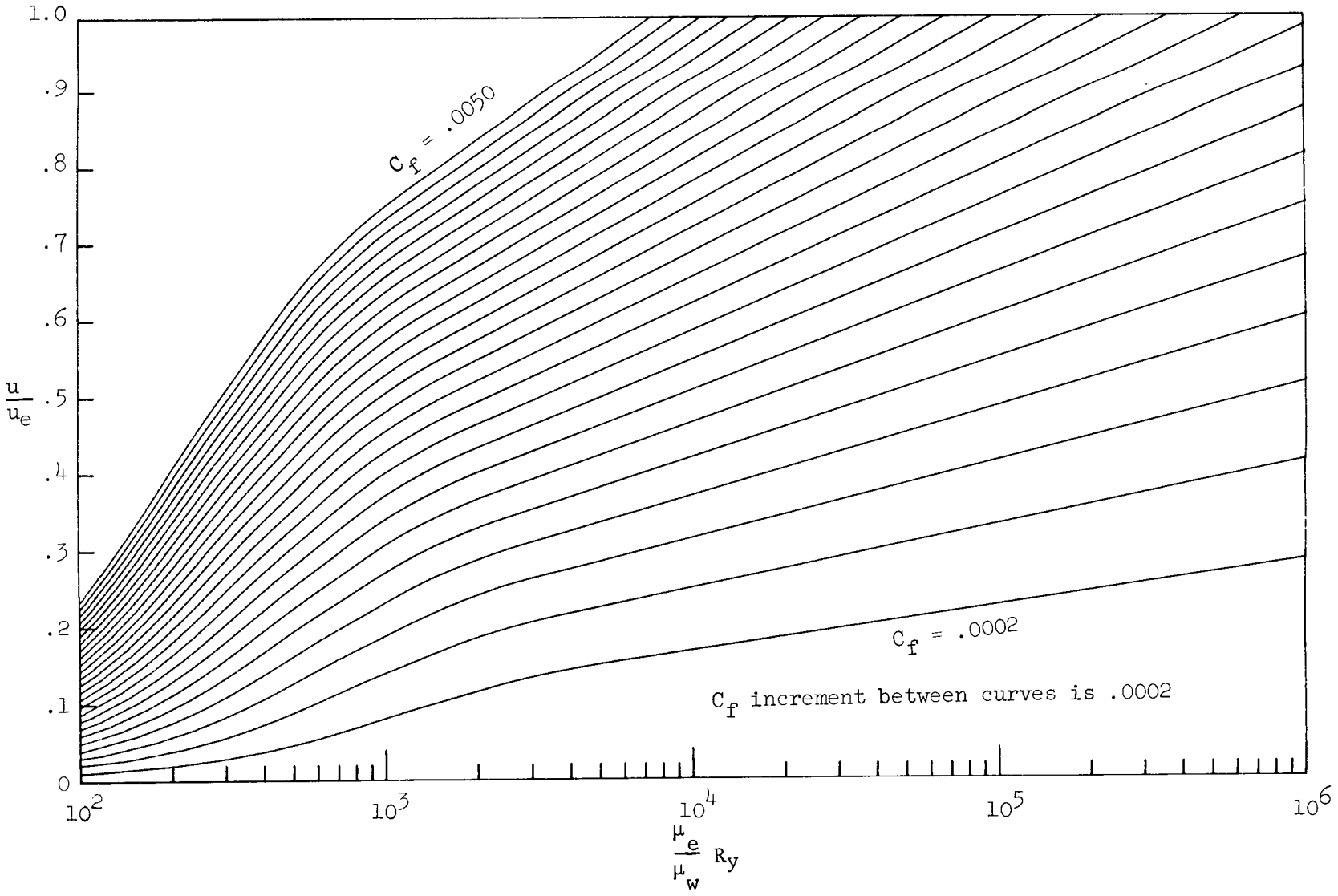

Figure 3.- Curves for interpolation of local skin-friction coefficients at $M_e = 0.40$.

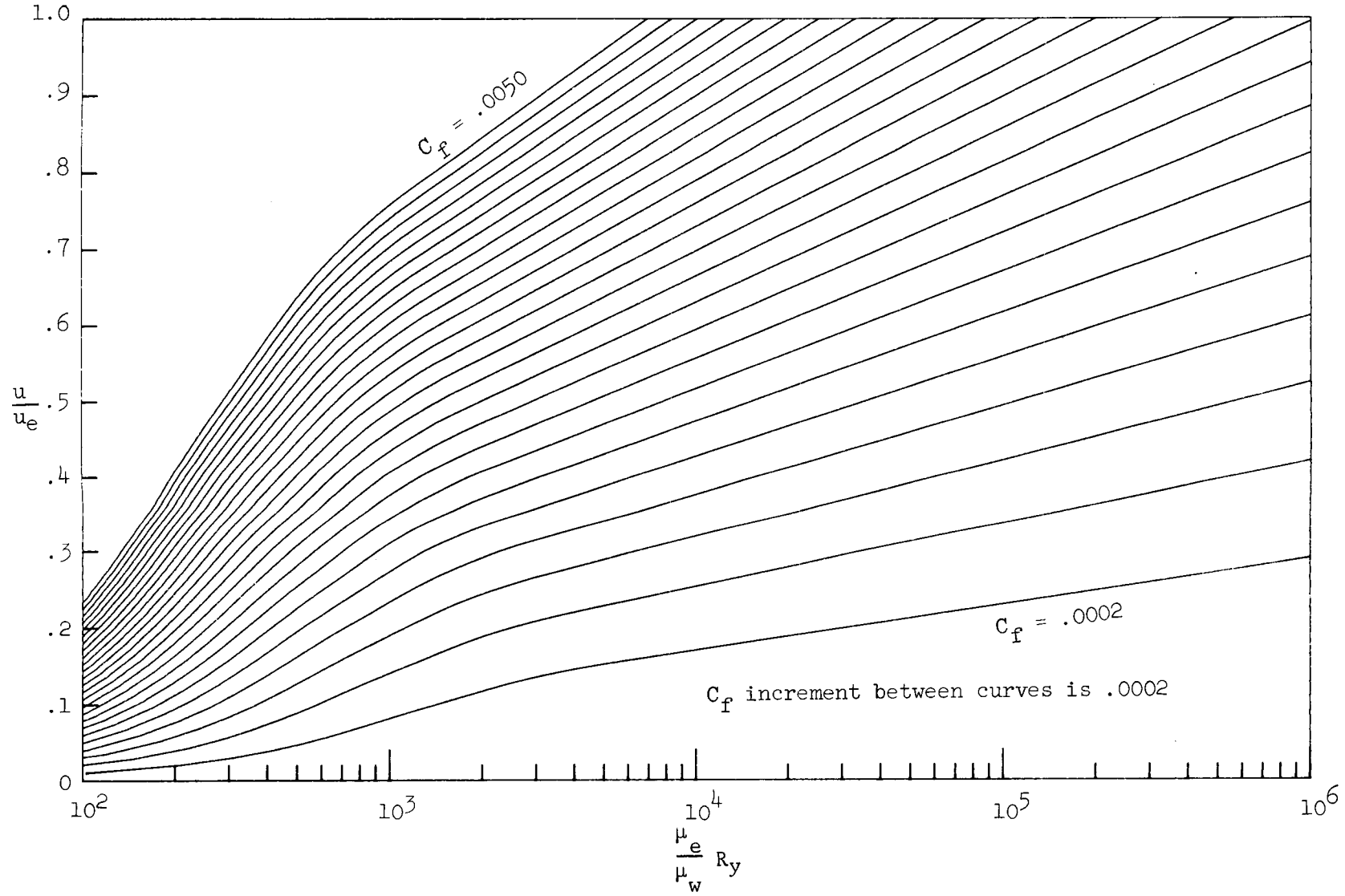

Figure 4.- Curves for interpolation of local skin-friction coefficients at $M_e = 0.60$.

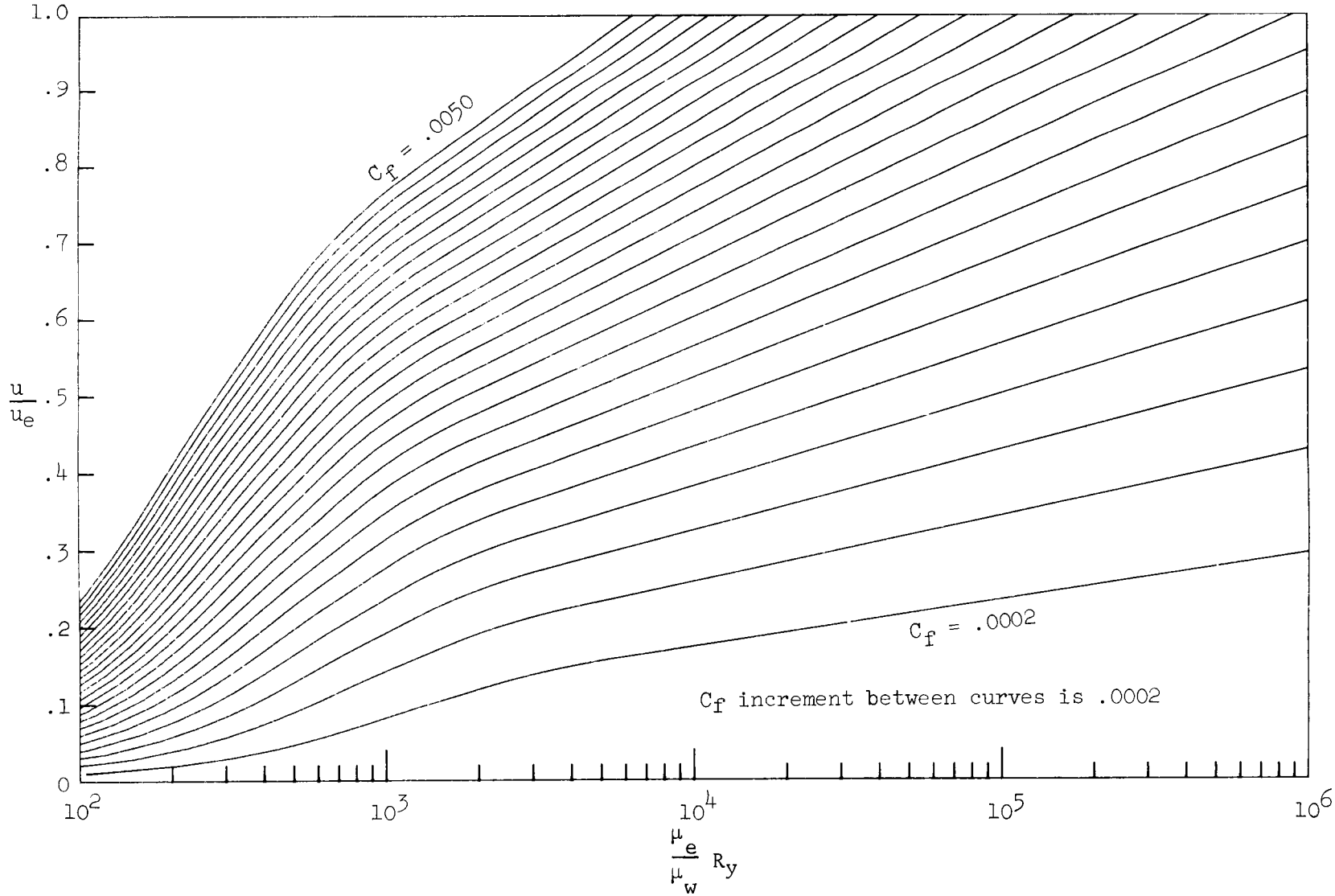

Figure 5.- Curves for interpolation of local skin-friction coefficients at $M_e = 0.80$.

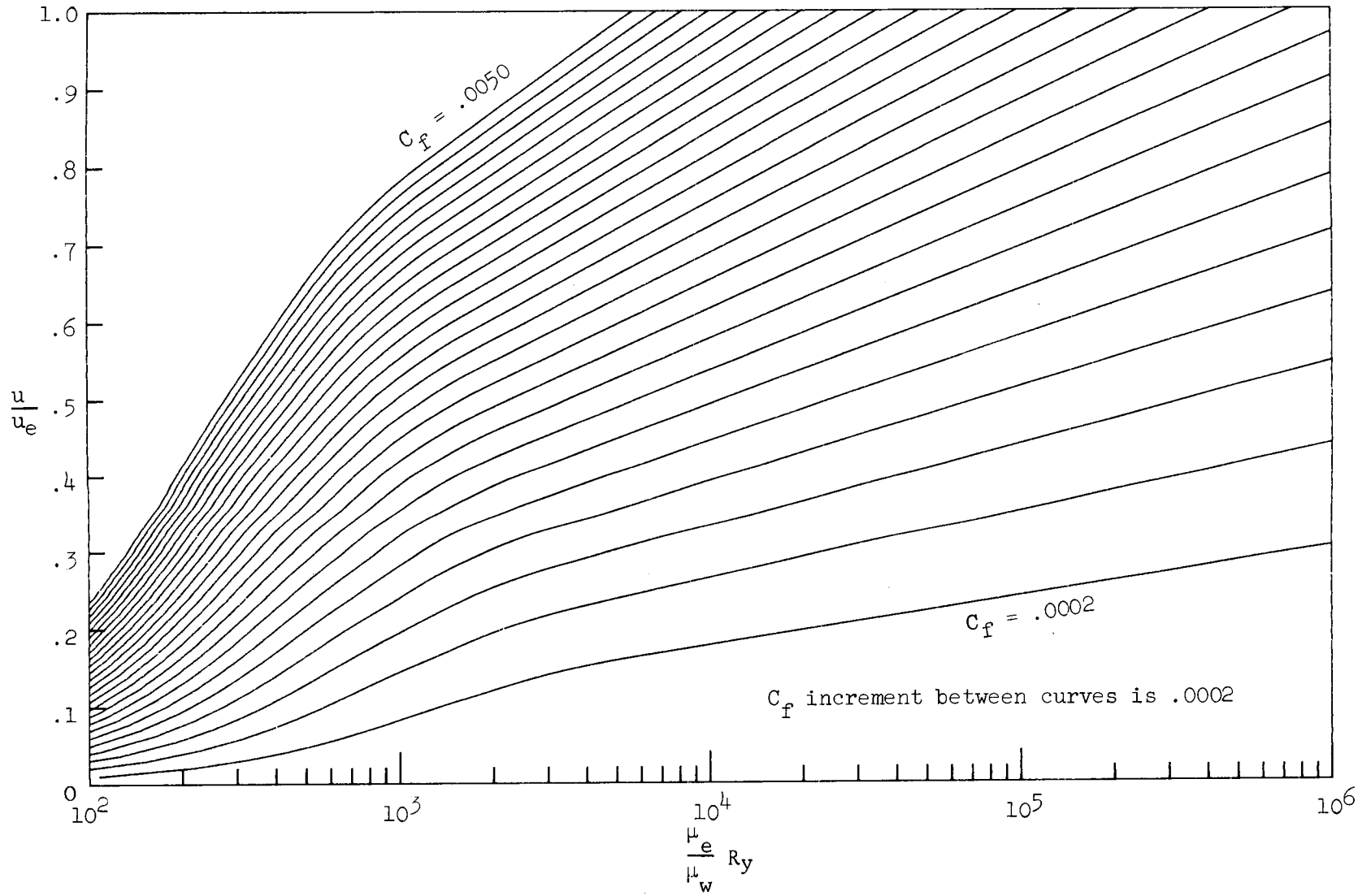

Figure 6.- Curves for interpolation of local skin-friction coefficients at $M_e = 1.00$.

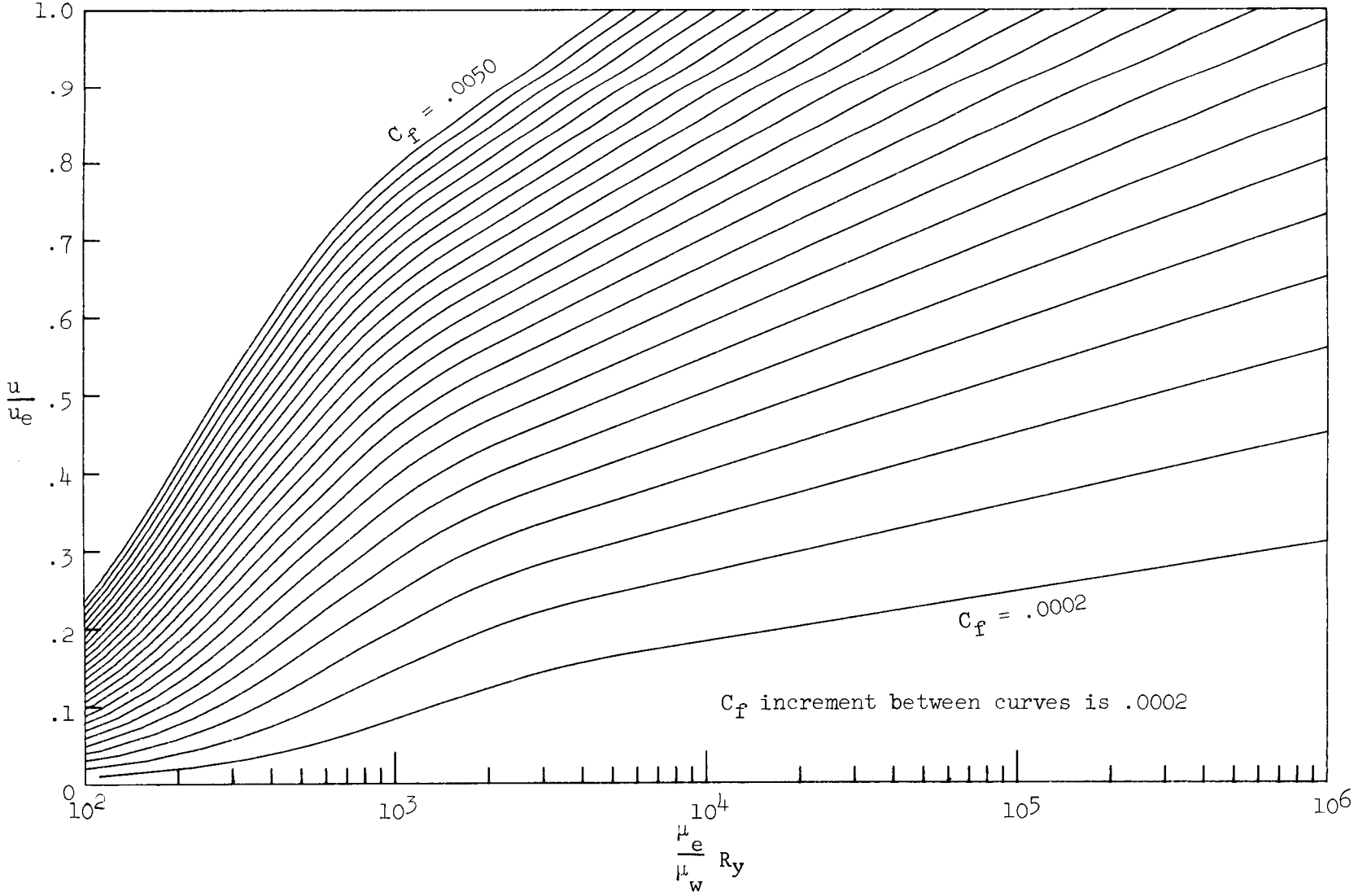

Figure 7.- Curves for interpolation of local skin-friction coefficients at $M_e = 1.20$.

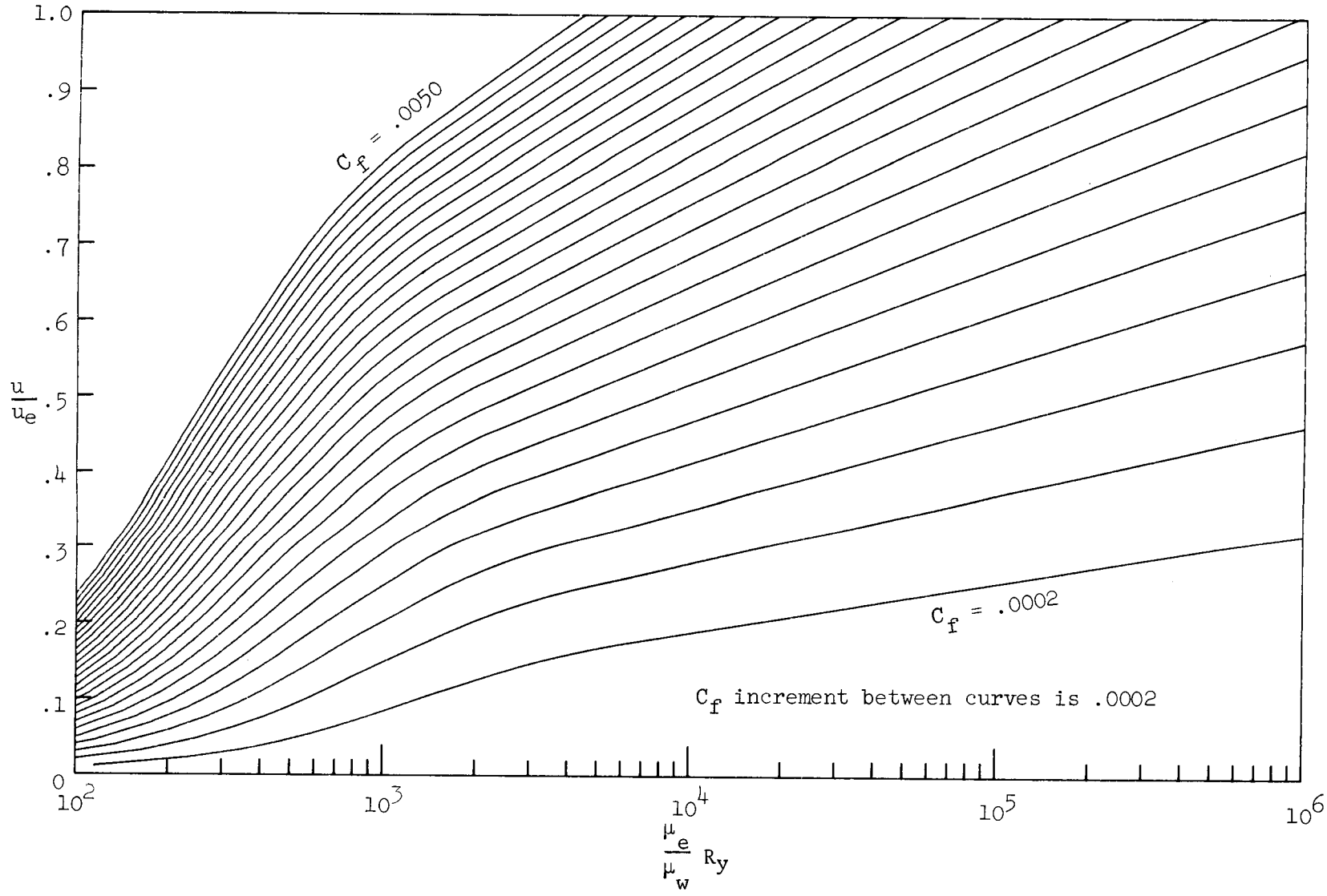

Figure 8.- Curves for interpolation of local skin-friction coefficients at $M_e = 1.40$.

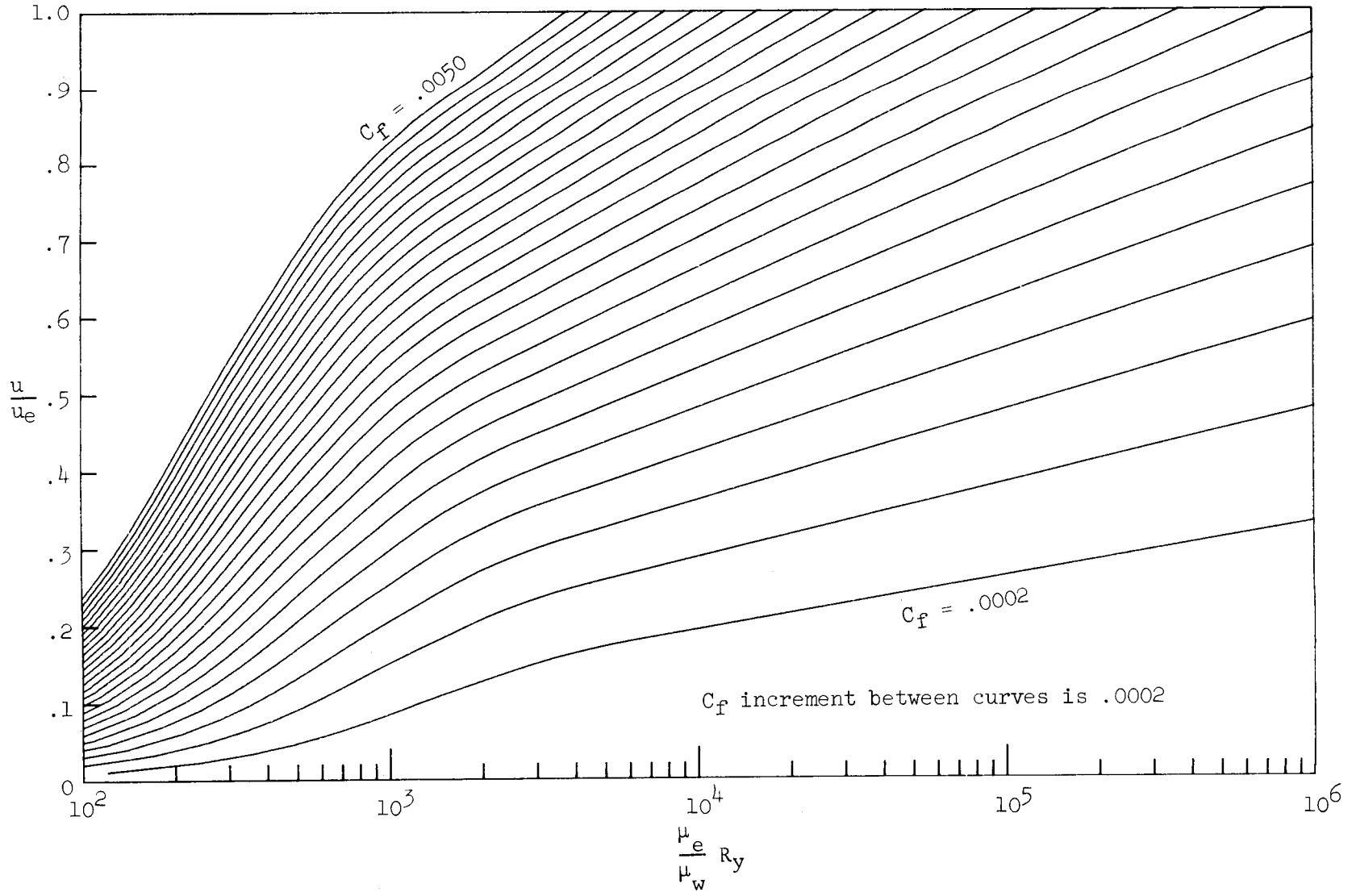

Figure 9.- Curves for interpolation of local skin-friction coefficients at $M_e = 1.60$.

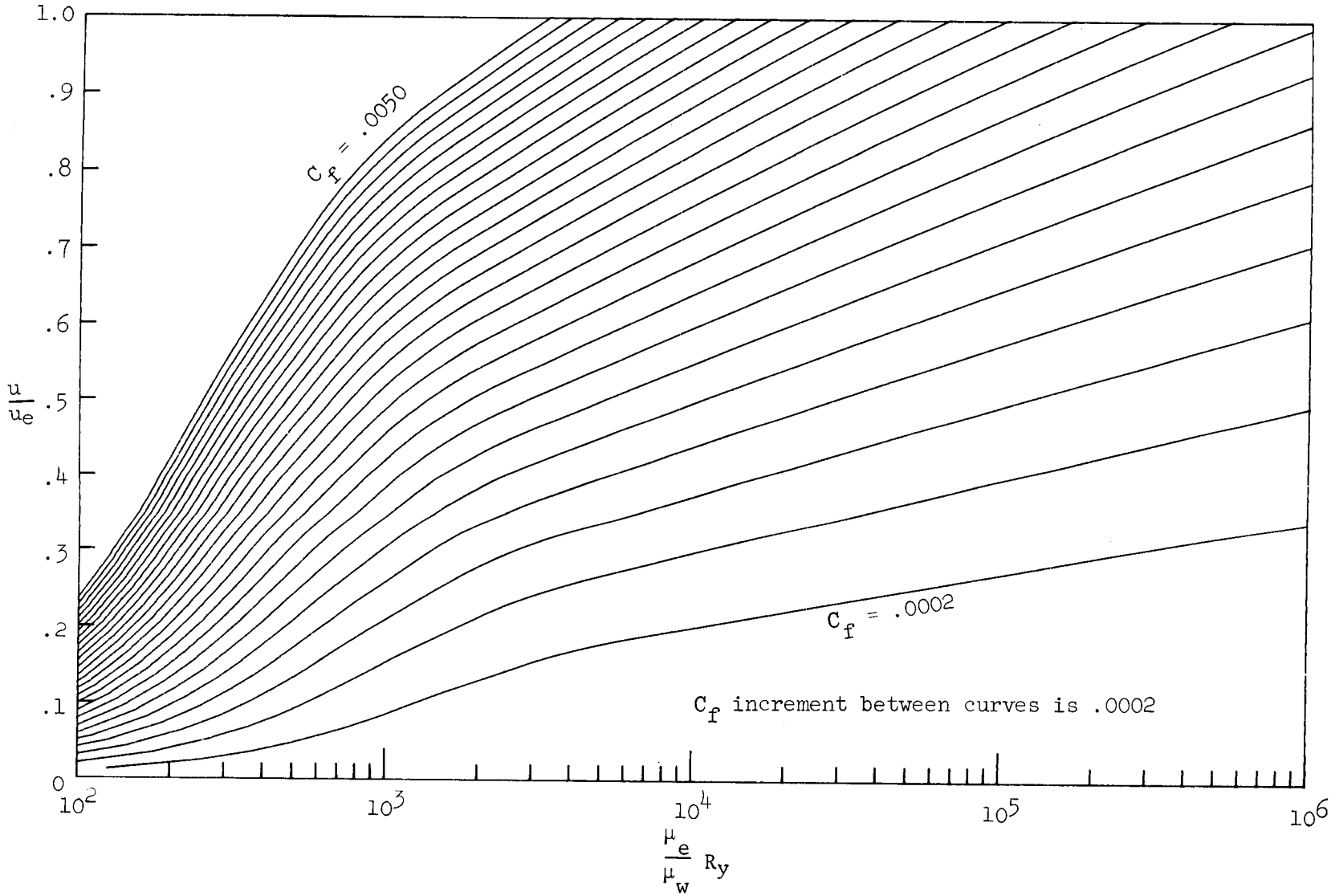

Figure 10.- Curves for interpolation of local skin-friction coefficients at $M_e = 1.80$.

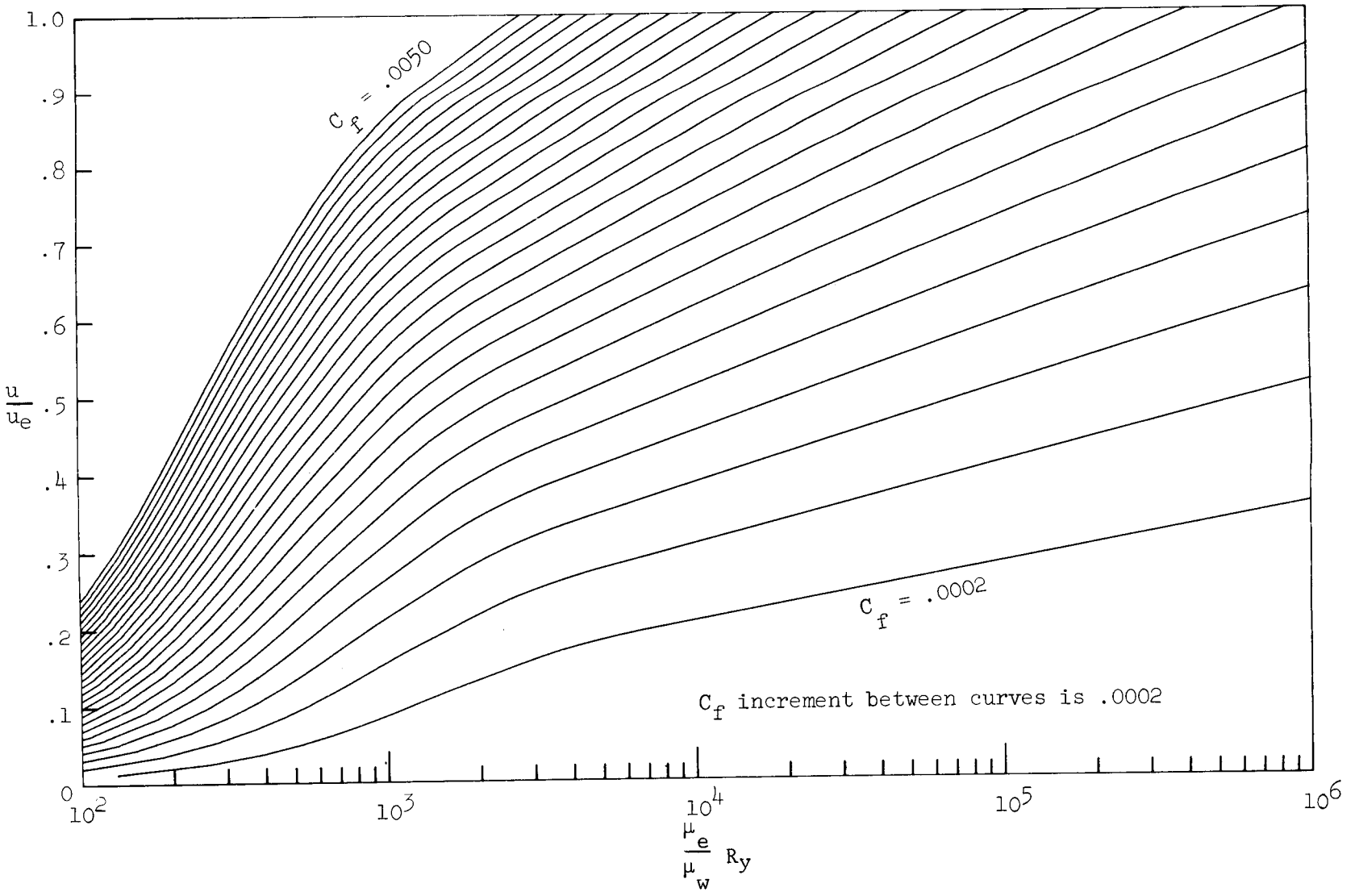

Figure 11.- Curves for interpolation of local skin-friction coefficients at $M_e = 2.00$.

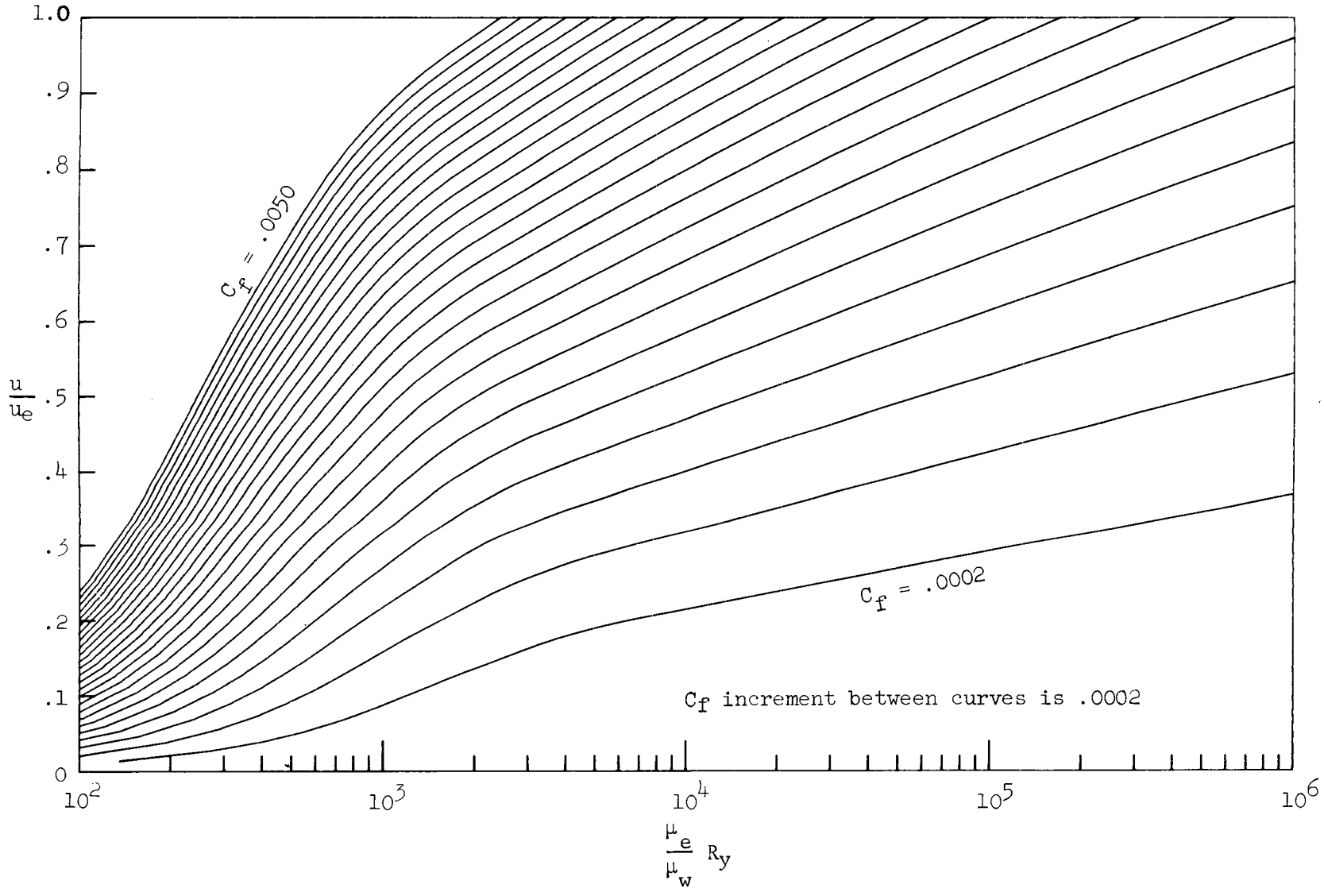

Figure 12.- Curves for interpolation of local skin-friction coefficients at $M_e = 2.20$.

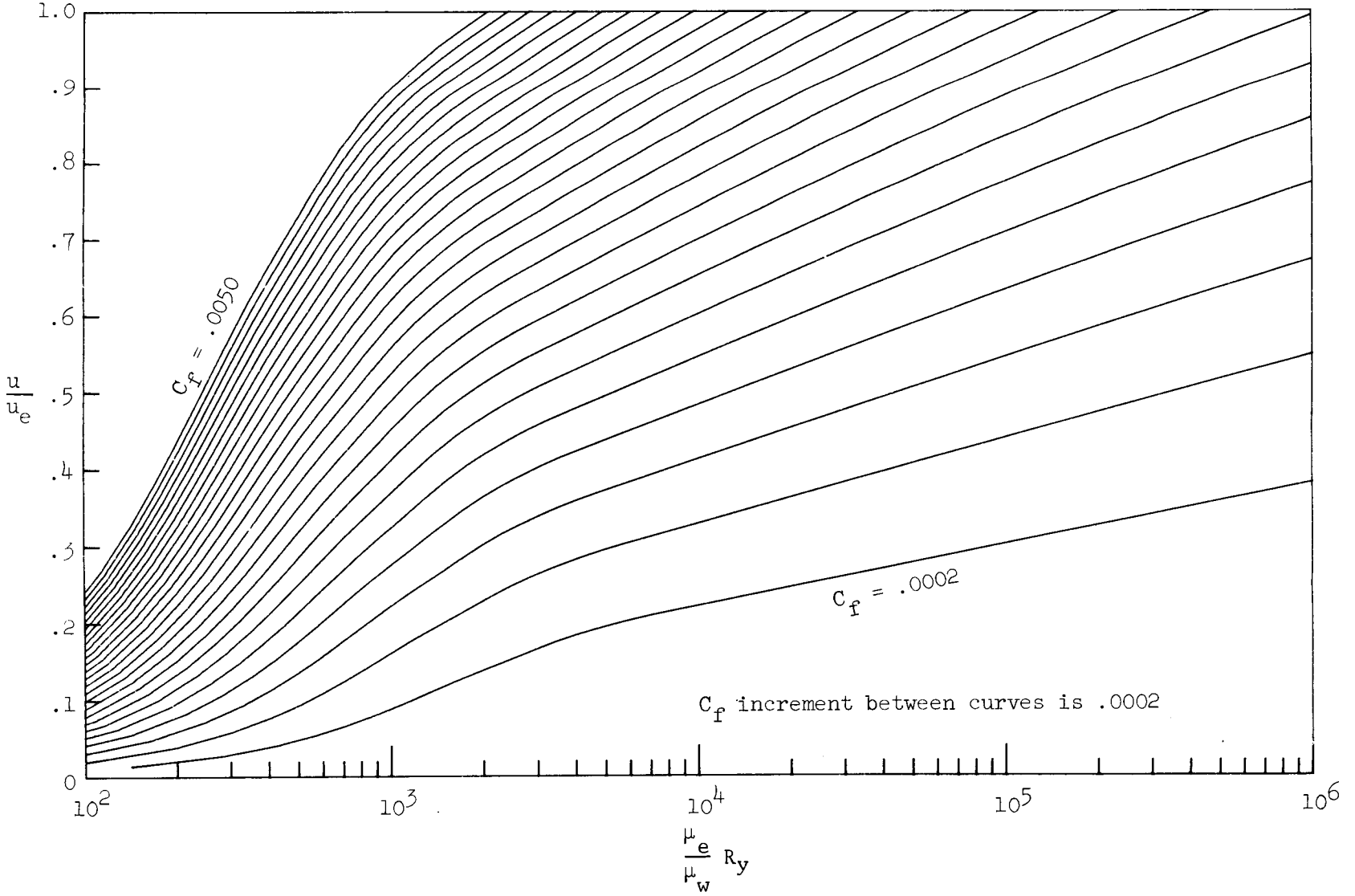

Figure 13.- Curves for interpolation of local skin-friction coefficients at $M_e = 2.40$.

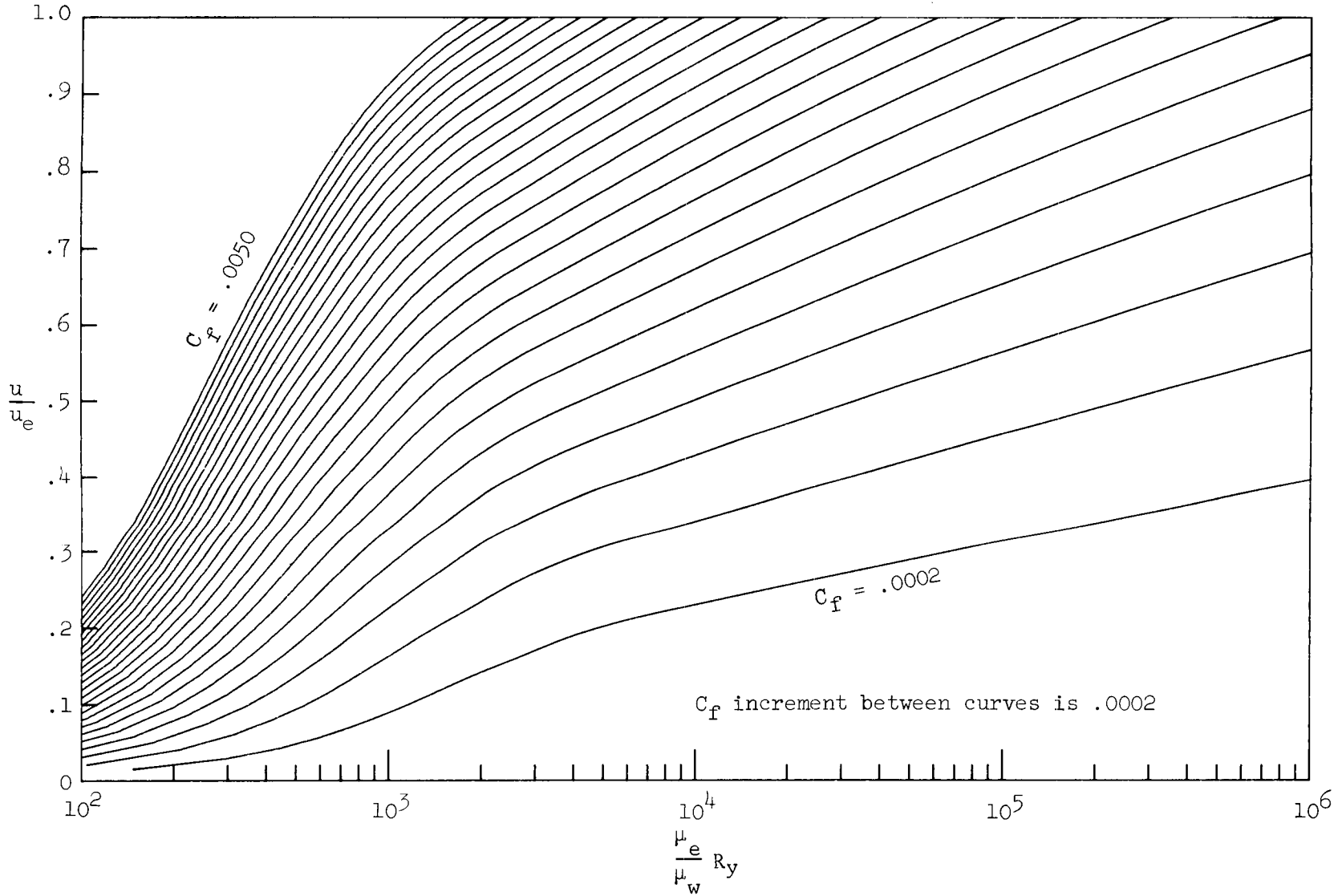

Figure 14.- Curves for interpolation of local skin-friction coefficients at $M_e = 2.60$.

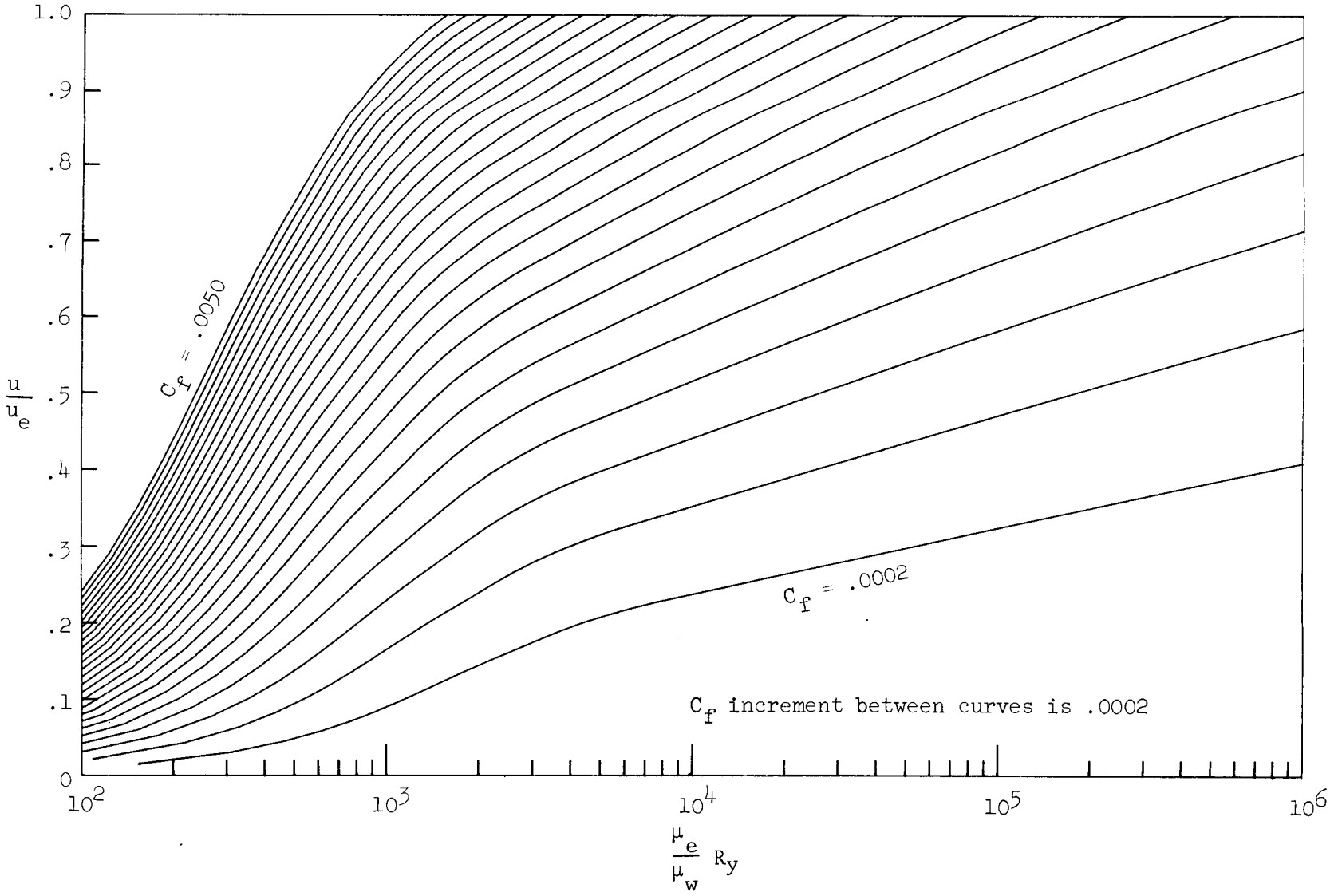

Figure 15.- Curves for interpolation of local skin-friction coefficients at $M_e = 2.80$.

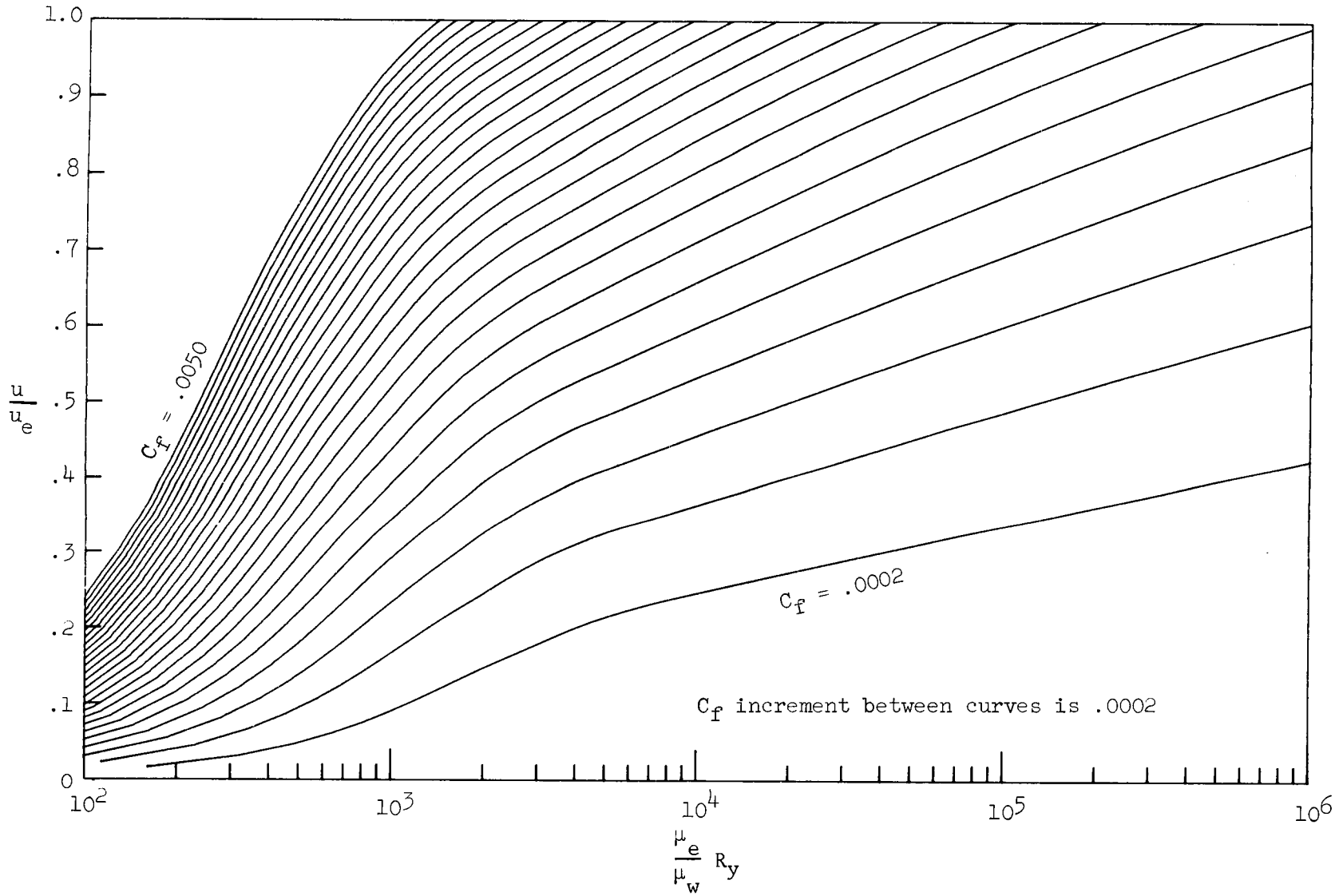

Figure 16.- Curves for interpolation of local skin-friction coefficients at $M_e = 3.00$.

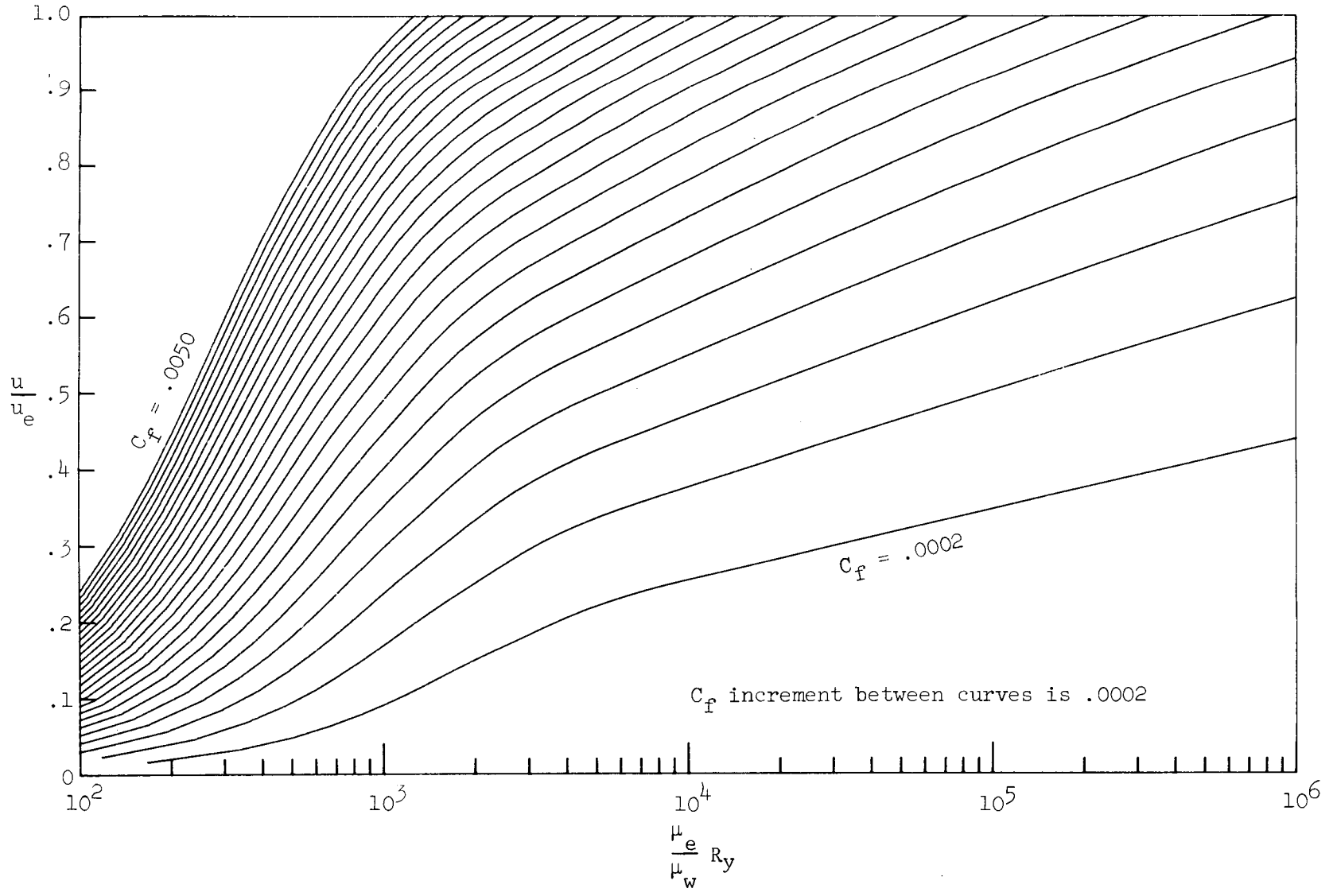

Figure 17.- Curves for interpolation of local skin-friction coefficients at $M_e = 3.20$.

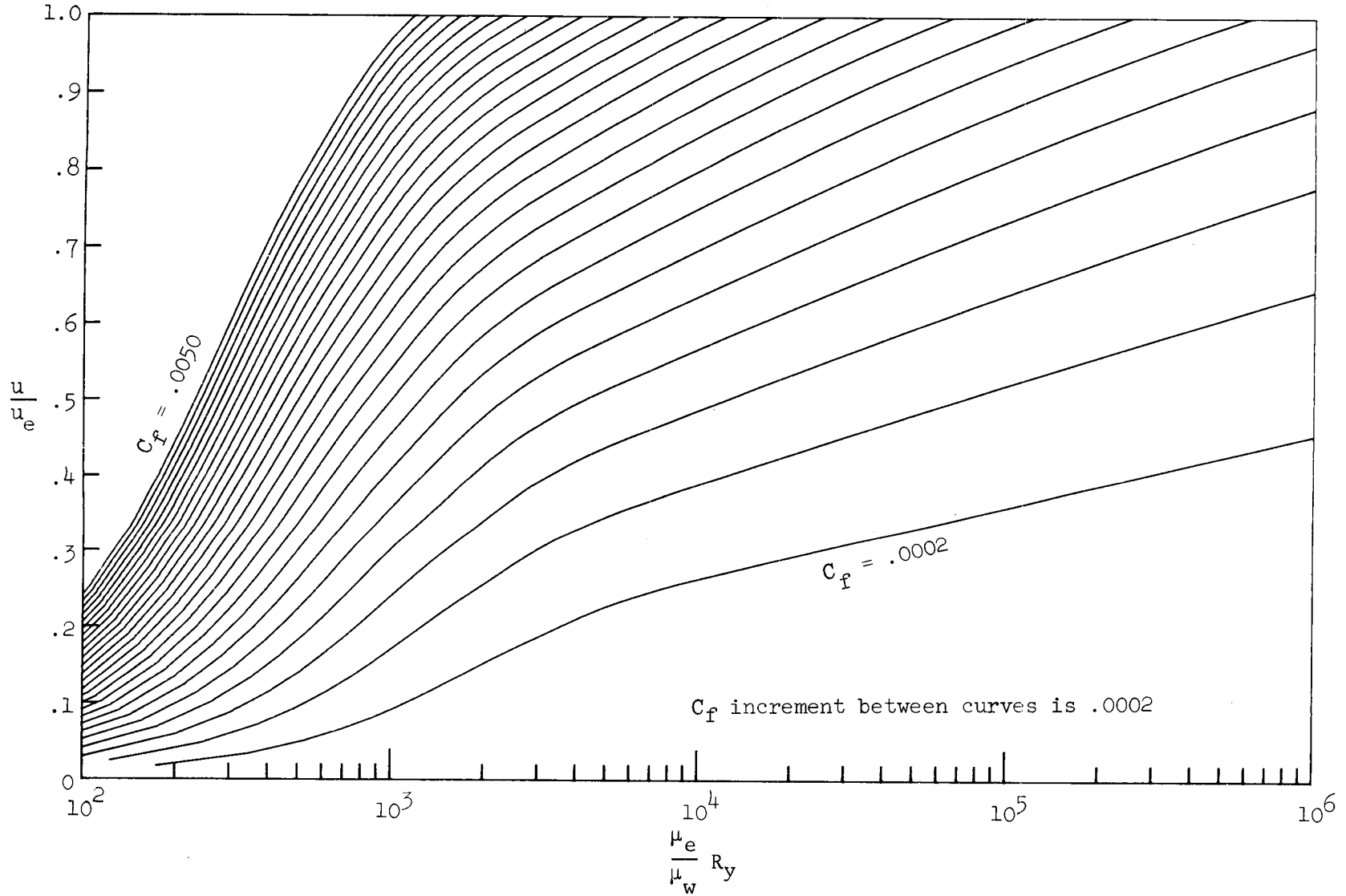

Figure 18.- Curves for interpolation of local skin-friction coefficients at $M_e = 3.40$.

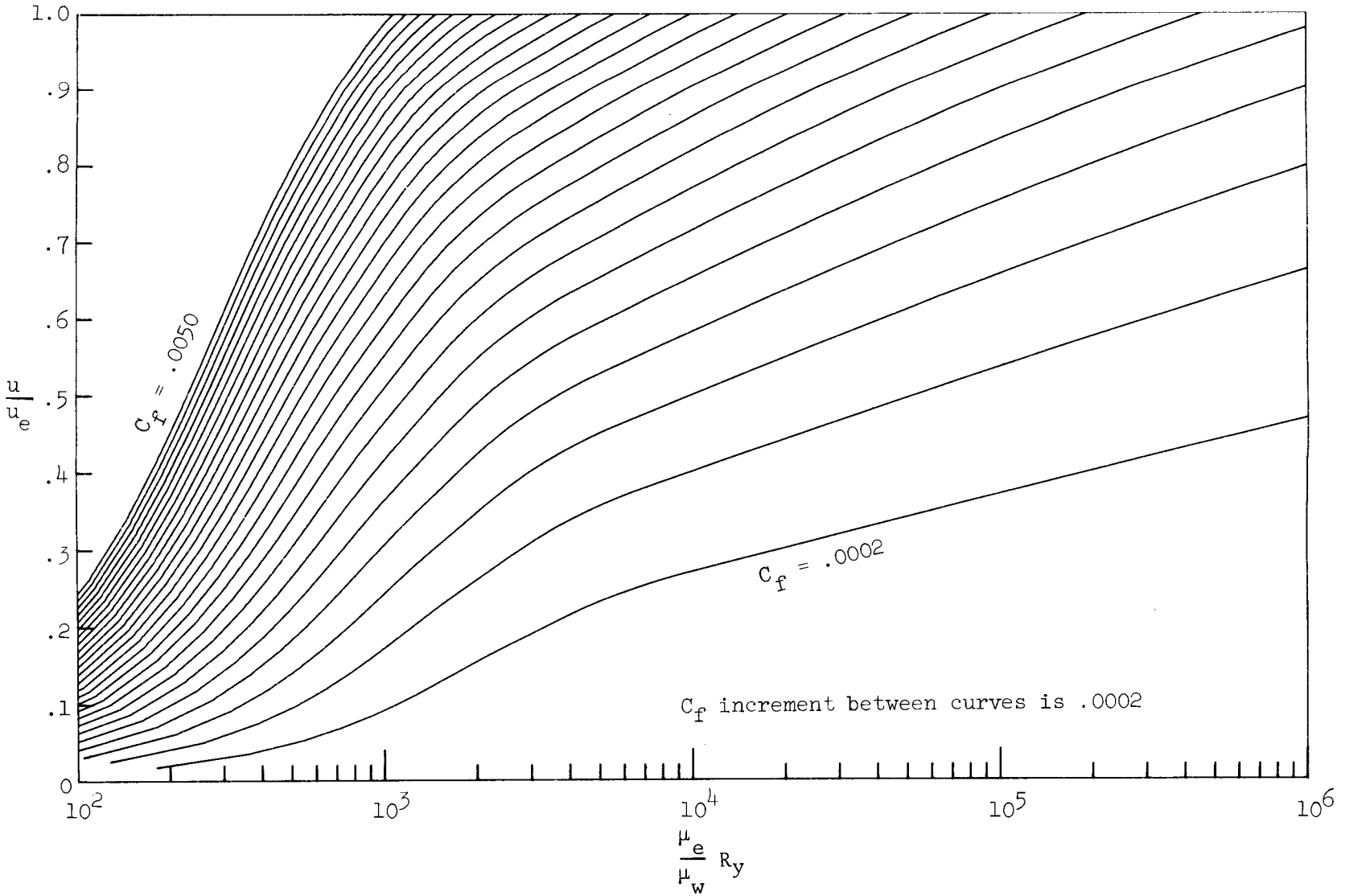

Figure 19.- Curves for interpolation of local skin-friction coefficients at $M_e = 3.60$.

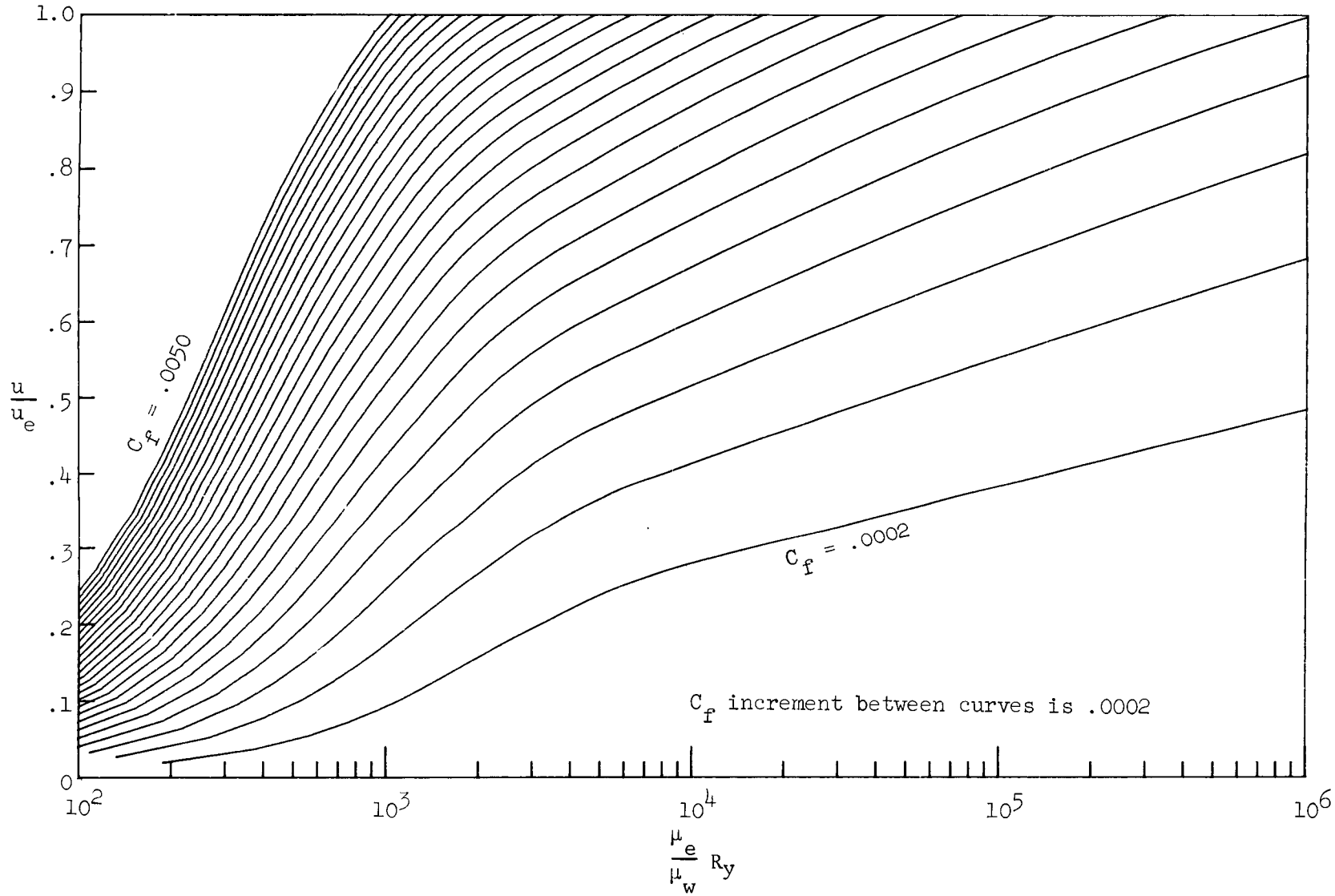

Figure 20.- Curves for interpolation of local skin-friction coefficients at $M_e = 3.80$.

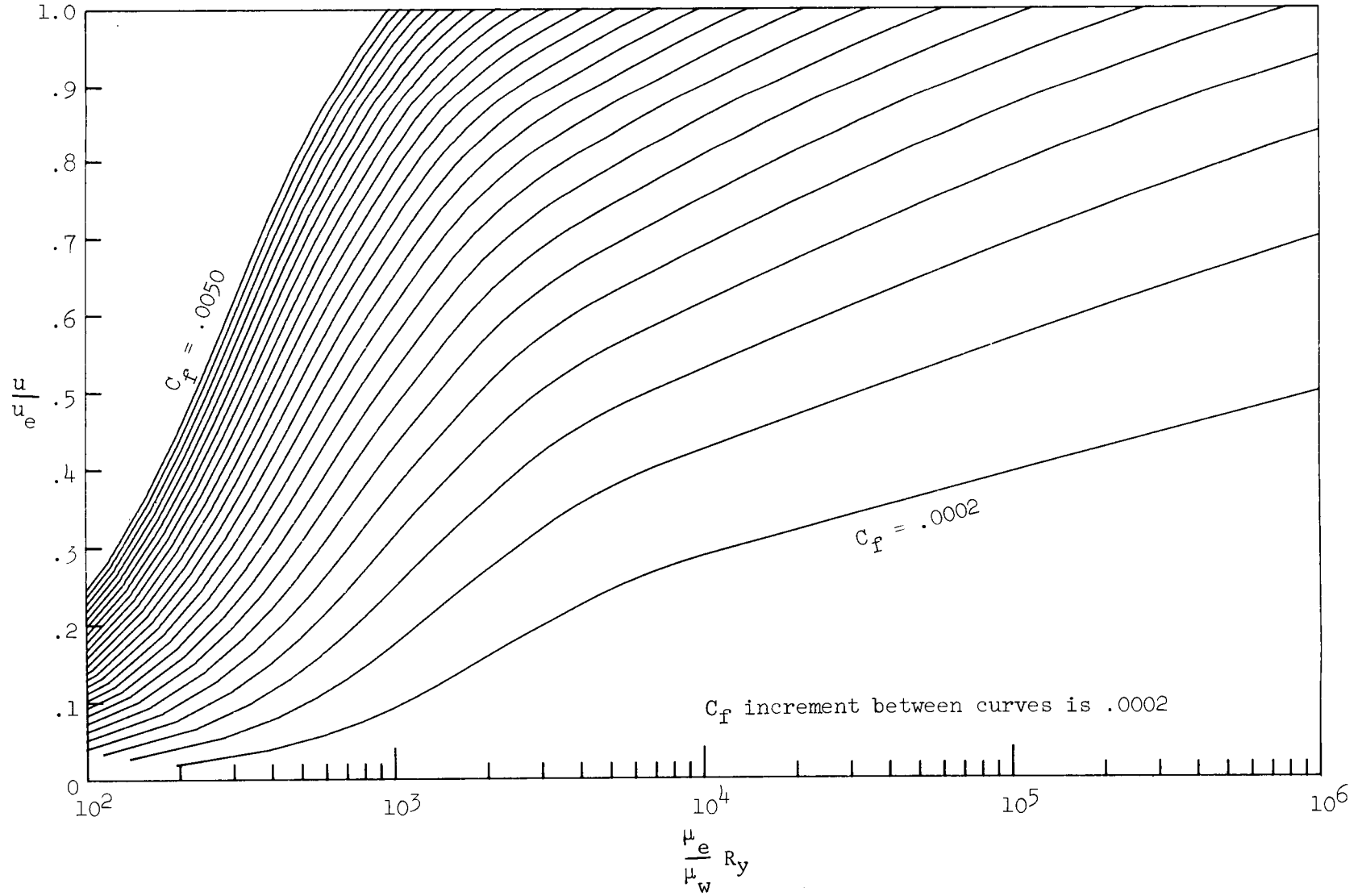

Figure 21.- Curves for interpolation of local skin-friction coefficients at $M_e = 4.00$.

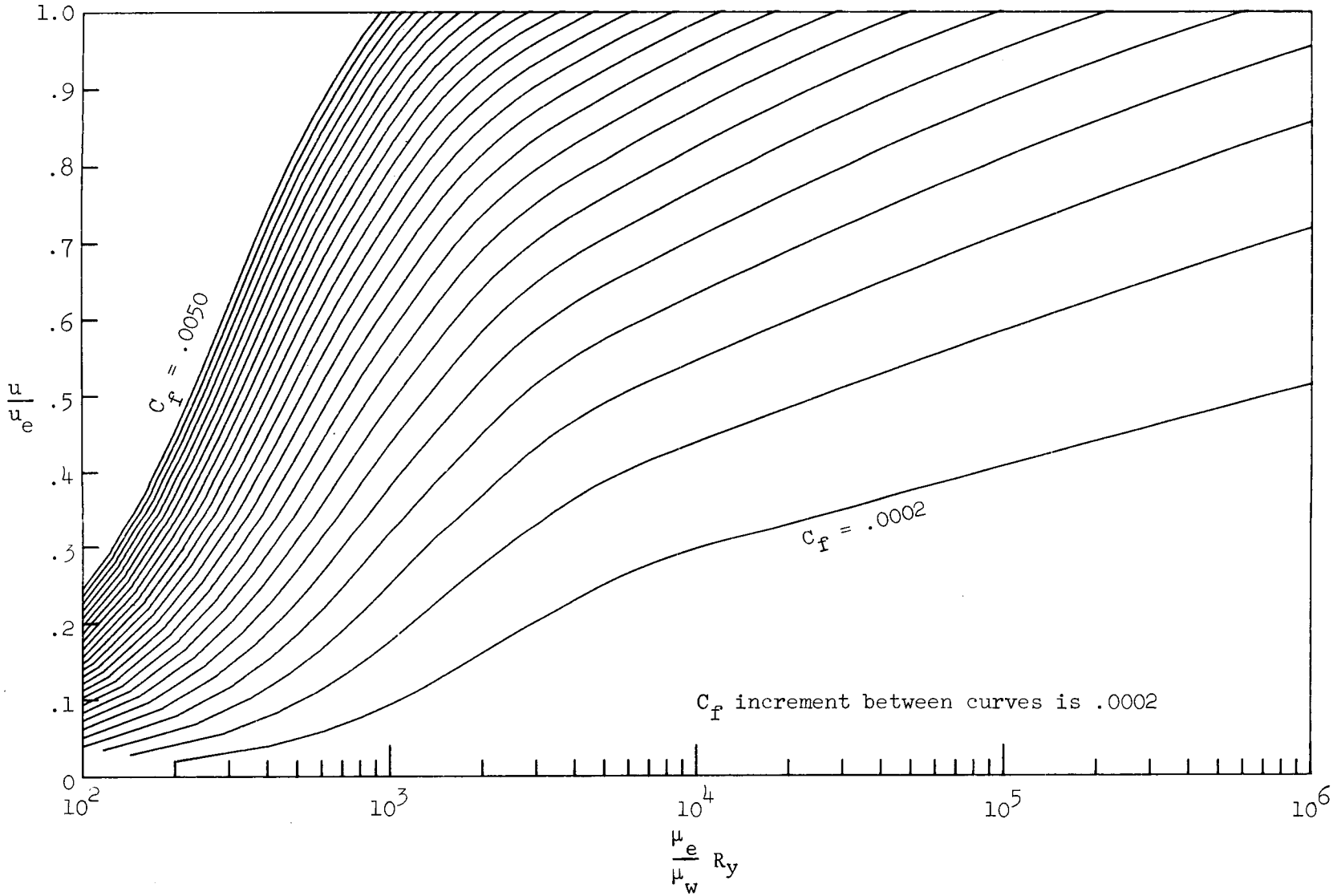

Figure 22.- Curves for interpolation of local skin-friction coefficients at $M_e = 4.20$.

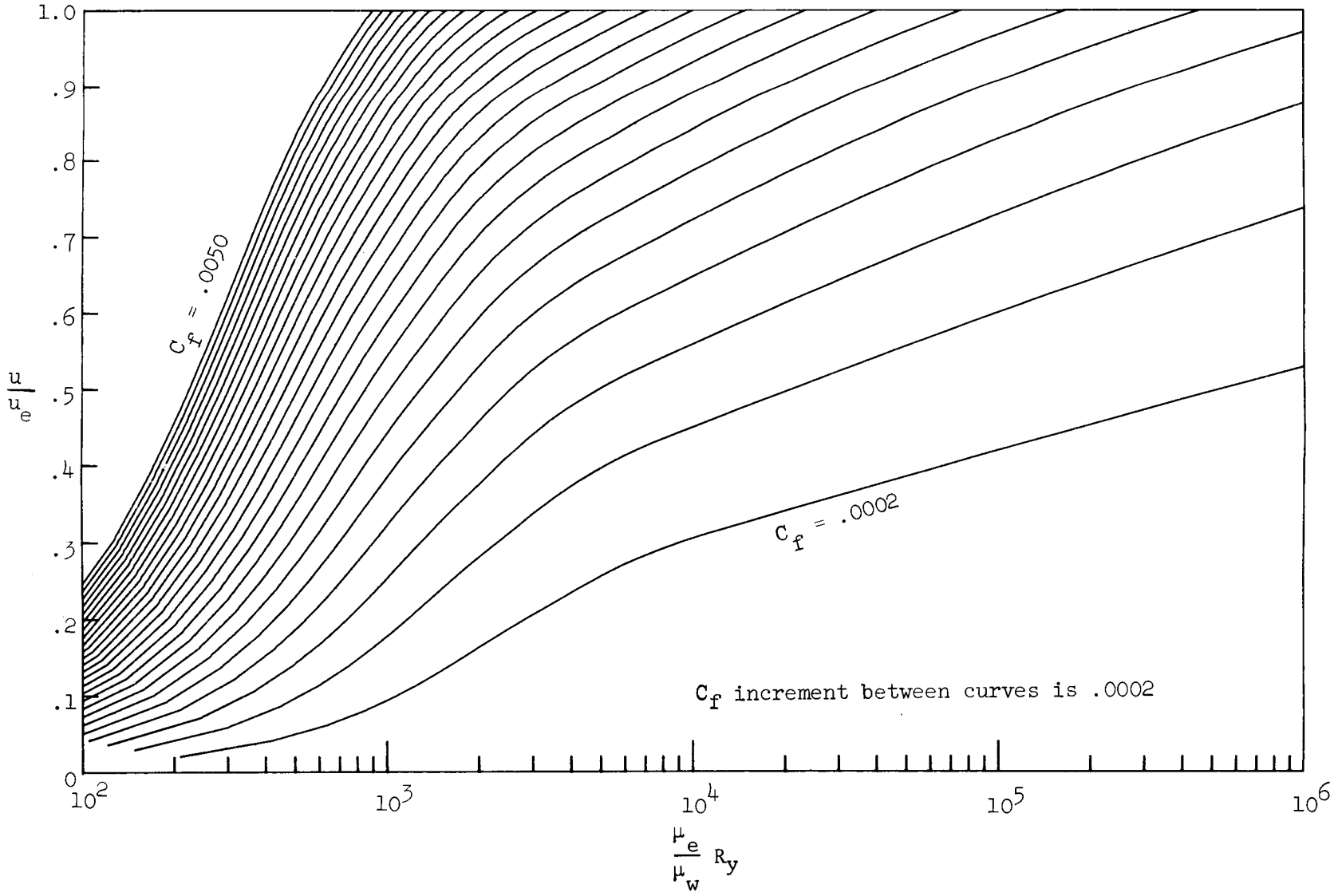

Figure 23.- Curves for interpolation of local skin-friction coefficients at $M_e = 4.40$.

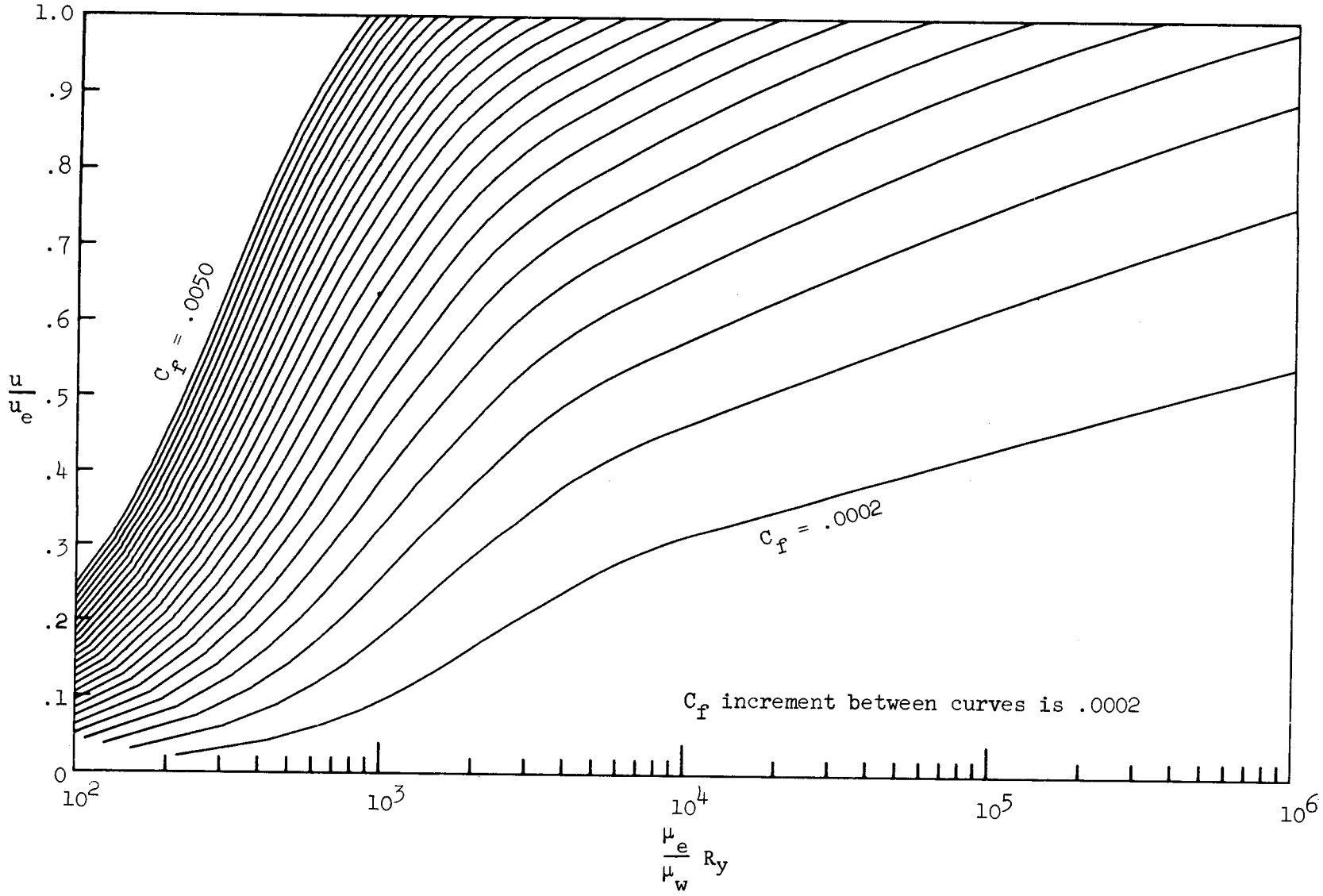

Figure 24.- Curves for interpolation of local skin-friction coefficients at $M_e = 4.60$.

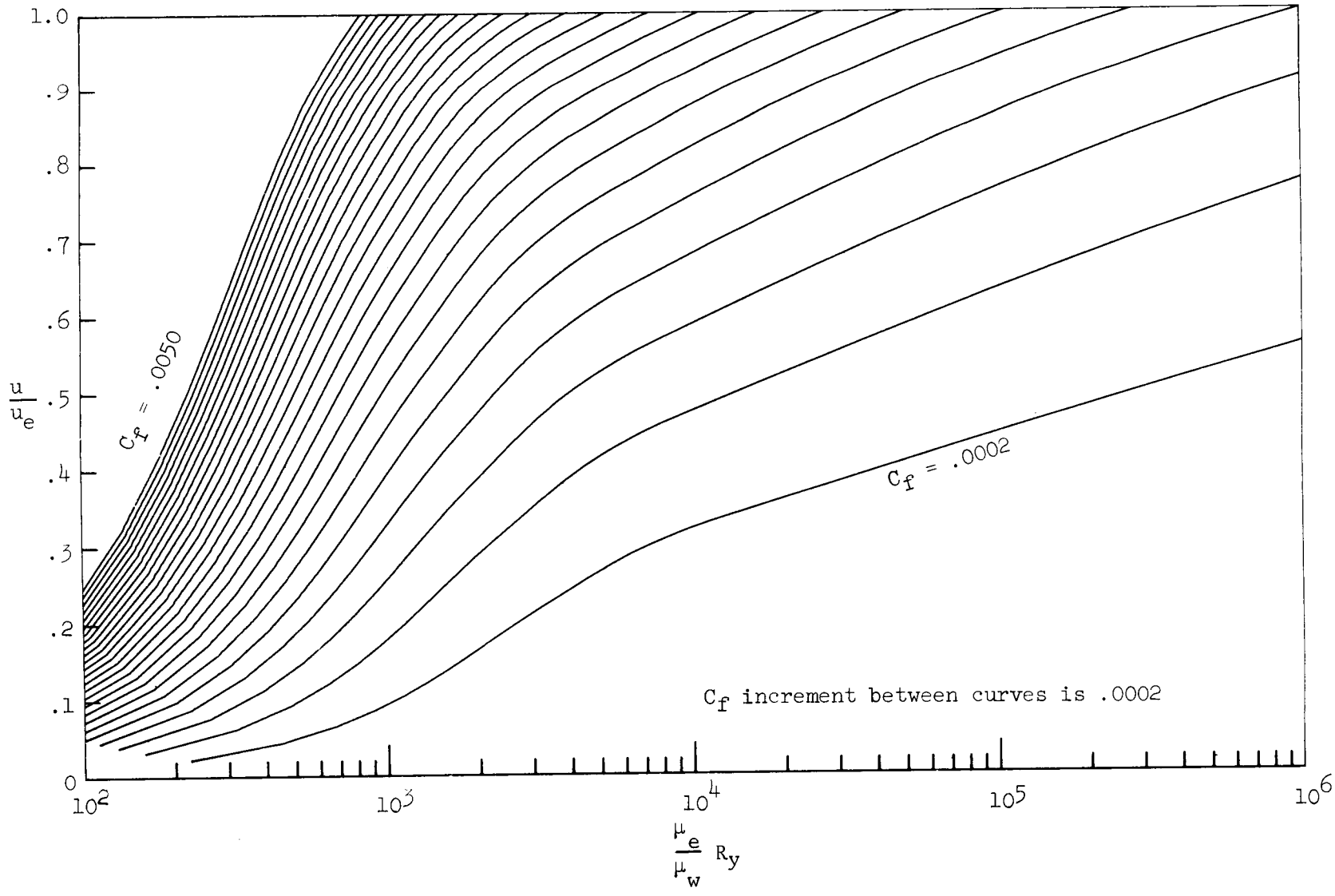

Figure 25.- Curves for interpolation of local skin-friction coefficients at $M_e = 4.80$.

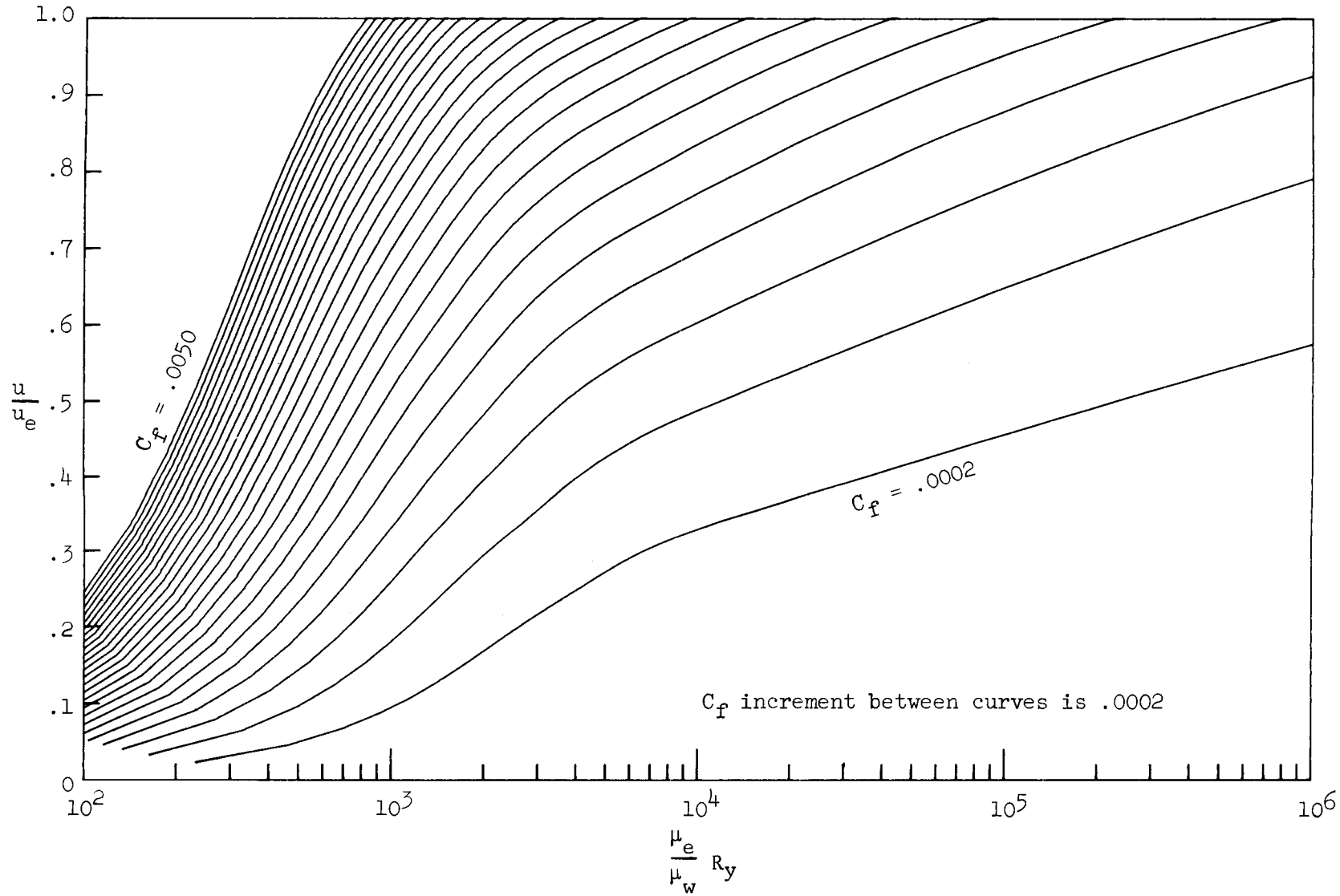

Figure 26.- Curves for interpolation of local skin-friction coefficients at $M_e = 5.00$.

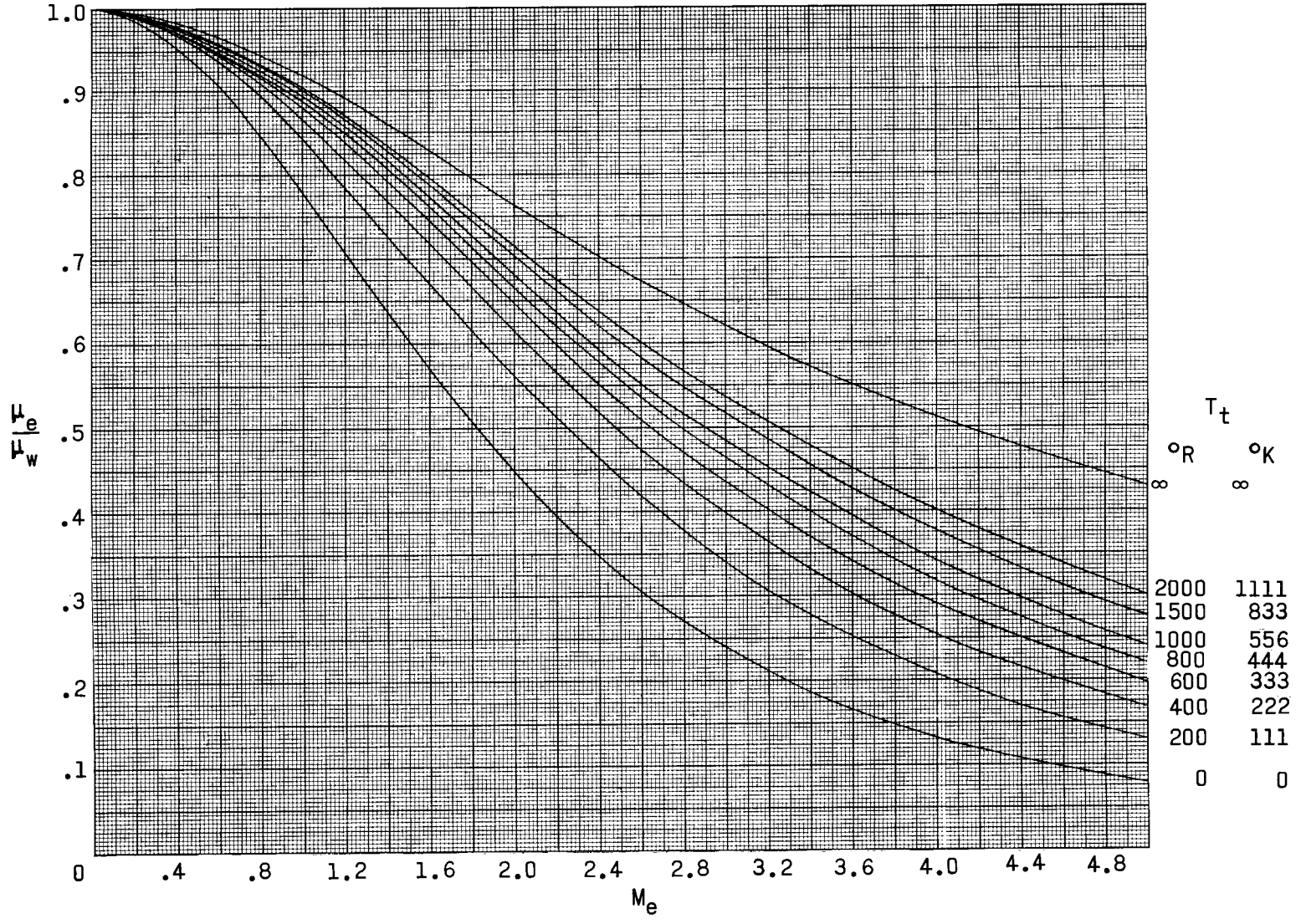

Figure 27.- Viscosity ratio from Sutherland viscosity law. $\frac{\mu_e}{\mu_w} = \frac{T_t + 199 + 39.8M_e^2 + 0.176M_e^2T_t}{\left(T_t + 199 + 39.8M_e^2\right)\left(1 + 0.176M_e^2\right)^{1.5}}$.

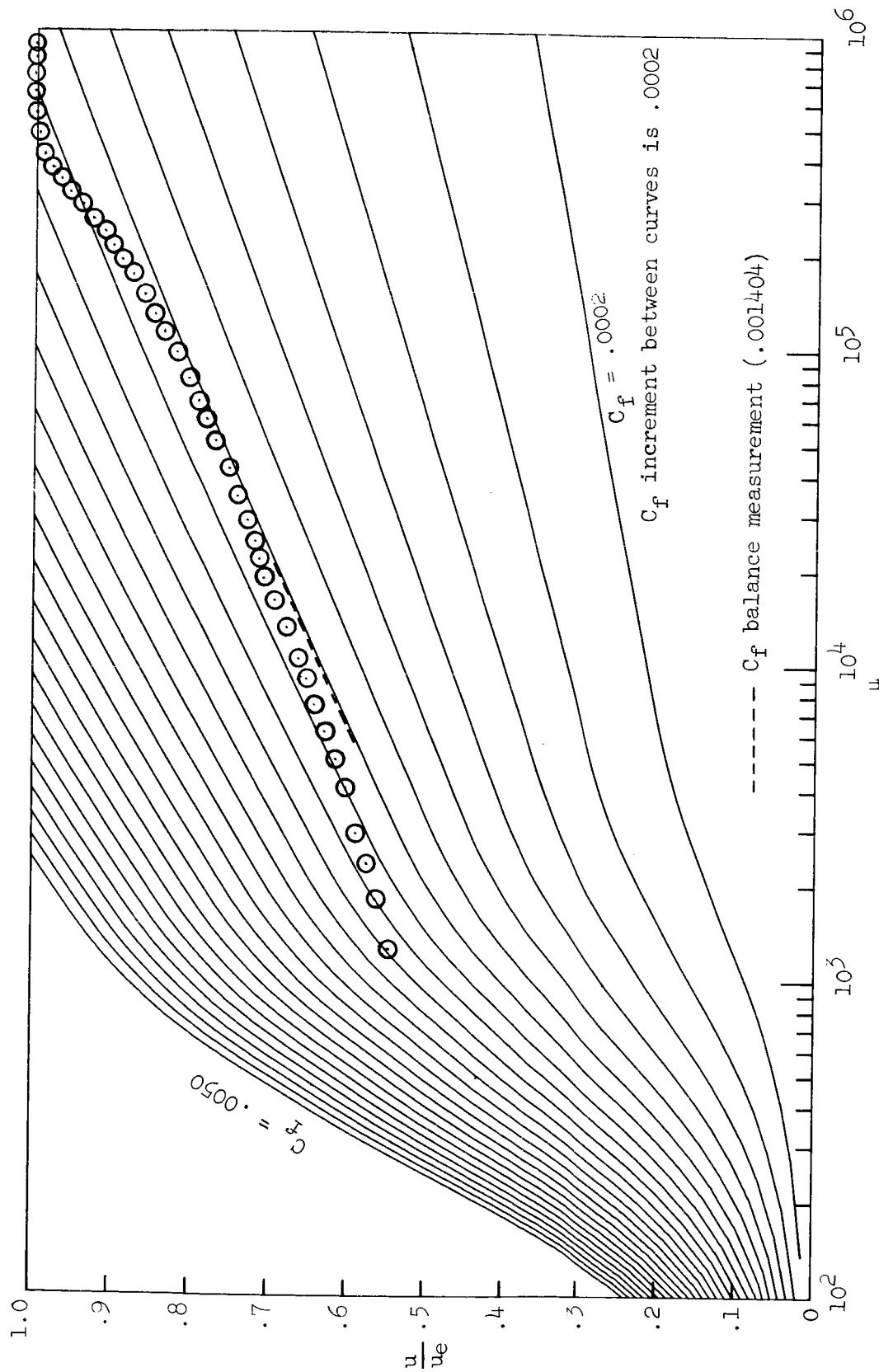

Figure 28.- Sample profile illustrating interpolation technique. M_e = 2.20.